

Article

Preclinical Study in Mouse Thymus and Thymocytes: Effects of Treatment with a Combination of Sodium Dichloroacetate and Sodium Valproate on Infectious Inflammation Pathways

Donatas Stakišaitis ^{1,2,*}, Linas Kapočius ¹, Evelina Kilimaitė ¹, Dovydas Gečys ³, Lina Šlekienė ¹, Ingrida Balnytė ¹, Jolita Palubinskienė ¹ and Vaiva Lesauskaitė ^{3,*}

¹ Department of Histology and Embryology, Medical Academy, Lithuanian University of Health Sciences, 44307 Kaunas, Lithuania; linas.kapocius@gmail.com (L.K.); lina.slekiene@lsmu.lt (L.Š.); ingrida.balnyte@lsmu.lt (I.B.); jolita.palubinskiene@lsmuni.lt (J.P.)

² Laboratory of Molecular Oncology, National Cancer Institute, 08660 Vilnius, Lithuania

³ Laboratory of Molecular Cardiology, Institute of Cardiology, Lithuanian University of Health Sciences, Sukileliu Ave., 50161 Kaunas, Lithuania; dovydas.gecys@lsmu.lt

* Correspondence: donatas.stakisaitis@lsmuni.lt (D.S.); vaiva.lesauskaite@lsmu.lt (V.L.); Tel.: +370-64641384 (D.S.); +370-861614001 (V.L.)



Citation: Stakišaitis, D.; Kapočius, L.; Kilimaitė, E.; Gečys, D.; Šlekienė, L.; Balnytė, I.; Palubinskienė, J.; Lesauskaitė, V. Preclinical Study in Mouse Thymus and Thymocytes: Effects of Treatment with a Combination of Sodium Dichloroacetate and Sodium Valproate on Infectious Inflammation Pathways. *Pharmaceutics* **2023**, *15*, 2715. <https://doi.org/10.3390/pharmaceutics15122715>

Academic Editors: Eva Torres-Sangiao and Erko O. Ylösmäki

Received: 29 October 2023

Revised: 17 November 2023

Accepted: 29 November 2023

Published: 30 November 2023

Correction Statement: This article has been republished with a minor change. The change does not affect the scientific content of the article and further details are available within the backmatter of the website version of this article.



Copyright: © 2023 by the authors. Licensee MDPI, Basel, Switzerland. This article is an open access article distributed under the terms and conditions of the Creative Commons Attribution (CC BY) license (<https://creativecommons.org/licenses/by/4.0/>).

Abstract: The research presents data from a preclinical study on the anti-inflammatory effects of a sodium dichloroacetate and sodium valproate combination (DCA–VPA). The 2-week treatment with a DCA 100 mg/kg/day and VPA 150 mg/kg/day combination solution in drinking water’s effects on the thymus weight, its cortex/medulla ratio, Hassall’s corpuscles (HCs) number in the thymus medulla, and the expression of inflammatory and immune-response-related genes in thymocytes of male Balb/c mice were studied. Two groups of mice aged 6–7 weeks were investigated: a control ($n = 12$) and a DCA–VPA-treated group ($n = 12$). The treatment did not affect the body weight gain ($p > 0.05$), the thymus weight ($p > 0.05$), the cortical/medulla ratio ($p > 0.05$), or the number of HCs ($p > 0.05$). Treatment significantly increased the Slc5a8 gene expression by 2.1-fold ($p < 0.05$). Gene sequence analysis revealed a significant effect on the expression of inflammation-related genes in thymocytes by significantly altering the expression of several genes related to the cytokine activity pathway, the inflammatory response pathway, and the Il17 signaling pathway in thymocytes. Data suggest that DCA–VPA exerts an anti-inflammatory effect by inhibiting the inflammatory mechanisms in the mouse thymocytes.

Keywords: inflammation; viral infection; bacterial infection; thymus; thymocytes; investigational medicinal preparation; genes

1. Introduction

The development of new drugs and the search for new therapeutic indications for registered medicines treating severe infections or cancer is an important research area of medicine. This article presents data from a preclinical study on the anti-inflammatory effects of a combination sodium dichloroacetate (DCA) and sodium valproate (VPA) preparation (DCA–VPA). VPA and DCA are known medicines with long-standing therapeutic experiences and established safety profiles, dosages, and blood concentrations. They are attractive candidates for studies to elucidate potential new therapeutic indications.

Severe infections disrupt systemic metabolism [1–3], which can cause death [4,5]. Mitochondria play a role in activating antiviral and anti-inflammatory mechanisms [6]. DCA and VPA investigational drugs have anti-inflammatory effects on viral and bacterial infections [7,8]. DCA is an inhibitor of pyruvate dehydrogenase kinase (PDK), inhibiting PDK activity and increasing the activity of pyruvate dehydrogenase (PDH) and its complex (PDHC) [9,10]. DCA is commonly used to treat diseases associated with mitochondrial

defects and increased congenital or acquired lactic acid production [11]. Various acquired metabolic and related immune dysfunction diseases are characterized by increased pathological expression of PDK, which inhibits PDHC, increases lactic acid production, causes its accumulation in tissues and blood, and releases inflammatory mediators [12,13]. PDK is a potential therapeutic target; its inhibition by DCA is meaningful in restoring immune and non-immune cell function [14–16]. PDH inactivation during infection is detected in peripheral blood mononuclear cells, skeletal muscle cells, vascular endothelial cells, and macrophages in severe infectious inflammation and sepsis [17,18]. The PDH subunit A1 (PDHA1)'s inactivation is associated with metabolic reprogramming and lactic acid overproduction [17,19]. Elevated blood lactic acid concentration is a biomarker of infection severity [12,20]. As a pro-inflammatory metabolite, lactic acid increases the production of pro-inflammatory cytokines [21,22]. Lactic acid, the end product of glycolysis, is an independent predictor of poor prognosis in sepsis, infectious coronavirus disease caused by SARS-CoV-2 virus (COVID-19), malaria, and other infections [23–26]. DCA regulates immune cells' anabolic and catabolic energy supply [8,27] and increases resistance to infection [28].

VPA is an antiepileptic drug [29] also being investigated as an immunomodulator [30], and it has been studied to treat various viral infections [31]. VPA is a histone deacetylase (HDAC) inhibitor [32]. HDAC inhibitors may be anti-inflammatory drugs [33]. VPA is a multifunctional regulator of cells of the innate and adaptive immune system and reduces macrophage infiltration in various models of inflammation [7], significantly down-regulated pro-inflammatory genes and macrophage infiltration in the kidney [34], reduced induced neutrophil influx in a Balb/c mouse model of lung inflammation, and induced a reduction in neutrophil infiltration in bronchoalveolar fluid [35]. The reduced ability of immune cells to induce a pro-inflammatory response after VPA treatment may suggest new therapeutic options for managing septic shock in Balb/c mice [36]. VPA attenuated the progression of Coxsackie B3 virus-induced myocarditis and the mortality of male BALB/c mice [37]; and it inhibited leukocyte migration into the peritoneal cavity by 92% in a peritonitis-induced model in male rats, reducing TNF- α , IL1 β , and IL6 levels with effects similar to indomethacin [38].

Pro-inflammatory immune cells derive most of their energy from aerobic glycolysis [39]. Glucose uptake and glycolysis are essential for the rapid growth and proliferation of virus-activated T cells [40,41]. Elevated glucose levels favor the progression of infection [42,43]. VPA and DCA reduce blood glucose levels in animals and humans [44–46].

VPA can activate Slc5a8, a sodium- and chloride-dependent monocarboxylate co-transporter encoded by the Slc5a8 gene (*Slc5a8*), u-regulating the expression of *Slc5a8* through DNA methylation [47,48]. Slc5a8 has a physiological function by transporting short-chain fatty acids into the cell and regulating mitochondrial metabolism; Slc5a8 is a transporter of DCA into the cell [49,50]. Slc5a8 regulates mitochondrial metabolism by participating in the mitochondrial β -oxidation pathway [51,52].

The thymus is the primary lymphoid organ where T lymphocytes mature and differentiate during the immune response. The thymus is responsible for generating T lymphocytes and is particularly vulnerable to infections [53]. Our previous research has shown that long-term monotherapy with DCA or VPA reduces the thymus weight of male Wistar rats [54,55].

This study aimed to investigate the effects of the DCA–VPA prolonged treatment of Balb/c mice on the thymus, its structure, and the expression of inflammation and immune-response-related genes in murine thymocytes. The objectives were to determine if the DCA–VPA treatment has an adverse effect on the mouse body and thymus weight, the effect on the expression of Hassall's corpuscles in the thymus medulla, and the effects on the expression of Slc5A8 and the cytokine activity pathway, inflammatory response pathway, and IL17 signaling pathway genes in male Balb/c mice thymocytes.

The study results show that the treatment with DCA–VPA of Balb/c male mice results in a synergistic effect of the components of the investigational product, which is mediated

by the VPA activation of DCA transport into thymocytes via the *Slc5a8* co-transporter gene's upregulation. This study has shown that DCA-VPA has an anti-inflammatory effect by inhibiting the expression of inflammation-promoting genes and increasing the expression of genes that inhibit infection-induced inflammation in murine thymocytes. This effect is related to inhibiting pro-inflammatory biological pathways. DCA-VPA is thus a suitable treatment option to reverse metabolic disturbances caused by inflammation.

2. Materials and Methods

2.1. The Investigational Medicinal Product

The investigational medicinal product is a combination of sodium dichloroacetate (DCA; Sigma-Aldrich, Steinheim, Germany) and sodium valproate (VPA; Sigma-Aldrich, Steinheim, Germany). The combination of these medicinal products (DCA-VPA) is patented by us as a new medicinal product for the treatment of cancer (official bulletin of the state patent bureau of the Republic of Lithuania, No. 6874, filing date 17 April 2020 <https://vpb.lrv.lt/uploads/vpb/documents/files/VPB-OB-Nr23-2021-12-10-1d.pdf> (accessed on 1 November 2023)); a European patent application is submitted (European patent application no. 21168796.7, filing date 16 April 2021 <https://register.epo.org/application?number=EP21168796> (accessed on 1 November 2023), as well as for the treatment of viral and bacterial infections (national patent application no. LT2023 532; 22 August 2023). Mice were treated with a drinking aqueous solution of the DCA-VPA combination (DCA 100 mg/kg and VPA 150 mg/kg/day) for two weeks. Considering the synergistic mechanism of action of DCA and VPA, the doses of DCA and VPA were half the doses we previously reported administered to animals treated with monotherapy [54,55].

2.2. The Groups of Mice and Experiments

The effect of DCA-VPA on the thymus gland of mice was investigated in two groups of male Balb/c mice aged 6–7 weeks: a control group ($n = 12$) and a matched group of male mice treated with a DCA-VPA solution ($n = 12$). The use of experimental animals for the studies was approved by the State Food and Veterinary Service of Lithuania (No. G2-198 of 16 March 2022). The animals were purchased from the Vivarium at the Veterinary Academy of the Lithuanian University of Health Sciences (Kaunas, Lithuania). The experiment was conducted at the Biological Research Center, Lithuanian University of Health Sciences (Kaunas, Lithuania). Animals were housed in standard colony cages with free access to food, warmth (21 ± 1 °C), humidity, and light/dark (12 h/12 h). Commercial pellet feed was provided ad libitum. The experiments followed laws and institutional animal care guidelines to avoid unnecessary animal suffering. After a 3-day acclimatization period, treatment of the animals with the DCA-VPA combination was initiated. The only source of drinking water was the DCA-VPA solution for the treated mice, while the control mice were supplied with fresh tap water; the DCA-VPA solution and water were available ad libitum to the animals. At the end of the experiment, 6 control and 6 treated mice were assigned to histological analysis of the thymus. Another 12 mice (6 control and 6 DCA-VPA-treated) were used to study *Slc5a8* expression, and RNR of 11 mice thymocytes (6 control and 5 DCA-VPA-treated) was used for the sequencing study (thymocyte RNR sequencing of 1 treated mouse was not tested due to insufficient RNA quality).

2.3. Thymus and Thymocyte Preparation

After the experiment, the animals were sacrificed in a 70% CO₂ chamber. To minimize the thymus contamination with red blood cells, the carotid arteries and the aorta were cut, and the animals exsanguinated. Upon killing the animals, their thymus was harvested, and the contaminating blood was removed by rinsing with Dulbecco's modified Eagle's medium (DMEM) (ThermoFisher Scientific, Bleiswijk, The Netherlands) supplemented with 2 mM L-glutamine (ThermoFisher Scientific, Vilnius, Lithuania) and penicillin-streptomycin solution (ThermoFisher Scientific, Vilnius, Lithuania). The weight of the thymus was evaluated. Thymus glands were collected for histomorphometric evaluation.

For the evaluation of isolated thymocytes, the thymus was processed by removing the connective tissue surrounding the gland. The thymus was minced and heavily pipetted several times. More significant cellular accumulations and connective tissue were removed by passing the suspension through two layers of surgical gauze. The lymphocyte suspension was washed of red blood cells by centrifugation in DMEM twice for 8 min each. The supernatant was removed. The isolated thymocytes were resuspended in DMEM (Thermo Fisher Scientific, Bleiswijk, The Netherlands) supplemented with 2 mM L-glutamine (Thermo Fisher Scientific, Vilnius, Lithuania) and penicillin–streptomycin solution (Thermo Fisher Scientific, Vilnius, Lithuania).

2.4. The Histological and Immunohistochemical Examination of the Thymus

The thymus samples were fixed in 10% neutral-buffered formalin, dehydrated, and embedded in paraffin; sections of 3 μm were obtained and stained with hematoxylin and eosin (H&E) (Sigma-Aldrich, Darmstadt, Germany). Immunohistochemical staining was performed on slices placed on glass slides coated with poly-L-lysine. Deparaffinization of sections in xylene and rehydration were followed by pretreatment with the antigen-retrieval solution Tris/EDTA buffer, pH 9, in a 95 °C pressure cooker for 20 min. Incubation with cytokeratin monoclonal antibodies (clone 34 β E12, dilution 1:100, Dako, Glostrup, Denmark) was used to identify high-molecular-weight cytokeratins (HMW CK). Each batch of slides was used for the positive control, and the negative control was achieved by omitting the primary antibody. The immunohistochemical reaction was revealed using an EnVision FLEX+, HRP kit (Dako, Glostrup, Denmark). EnVision FLEX Hematoxylin (Dako, Glostrup, Denmark) was used to counterstain the sections. The micro-morphometric and -morphologic evaluation of the samples was performed with an OLYMPUS BX53F microscope (Tokyo, Japan) equipped with a digital camera (Q-imaging, Surrey, BC, Canada) and using the Image-Pro Plus version 7.0 software (Media Cybernetics, Rockville, MD, USA). The thymus' entire area and the cortical and medullary parts were measured, and the cortical/medullary parts ratio was calculated. Both lobes were scanned with the scanning microscope and measured using Image-Pro Plus version 7.0 software. The cortical and medullary parts were evaluated by measuring the total area (mm^2) of each of the two lobes seen in one section. Hassall's corpuscles (HCs) in the thymic medulla were assessed. Even a tiny cluster of epithelial reticular cells and a concentric arrangement of the cells was counted as an HC. Two independent histologists counted the number of HCs in the thymus medullary portion (the resulting number of HCs did not differ by more than 5% between the two investigators), and the results of the study are presented as the mean number of HCs per mm^2 of the thymic area in each group.

2.5. Extraction of Total RNA from Thymocytes

A commercial TRIzol™ Plus RNA Purification Kit (Invitrogen™, Thermo Fisher Scientific, Bleiswijk, The Netherlands) was used to extract total RNA from the cells. Total RNA was quantified using a NanoDrop 2000 spectrophotometer (Thermo Scientific, Waltham, MA, USA). The integrity of the total RNA (RIN) was evaluated on an Agilent 2100 device (Agilent Technologies, Santa Clara, CA, USA) using an RNA 6000 Nano kit (Agilent Technologies, Santa Clara, CA, USA). Total RNA sample preparations were aliquoted and stored at -80 °C until subsequent downstream analysis.

2.6. Evaluation of the *Slc5a8* Expression in Thymocytes

Total RNA was reverse transcribed using a High-Capacity cDNA Reverse Transcription Kit (Applied Biosystems™, Thermo Fisher Scientific, Bleiswijk, The Netherlands) supplemented with RNaseOUT™ Recombinant Ribonuclease Inhibitor (Invitrogen™, Thermo Fisher Scientific, Bleiswijk, The Netherlands). The real-time polymerase chain reaction (PCR) for *Slc5a8* (TaqMan Assay ID: mm00520629_m1) was performed using TaqMan chemistry (Applied Biosystems™, Thermo Fisher Scientific, Bleiswijk, The Netherlands), according to manufacturer's instructions on a 7900 Real-Time PCR System (Applied

Biosystems™ Thermo Scientific, Carlsbad, CA, USA). Samples were run in triplicate. The glyceraldehyde-3-phosphate dehydrogenase gene (*Gapdh*) was used as a reference (TaqMan Assay ID: mm99999915_g1). Gene expression alterations were analyzed using the $2^{-\Delta\Delta Ct}$ method [56].

2.7. Next-Generation Sequencing

According to the manufacturer's instructions, next-generation sequencing (NGS) libraries were prepared using the QIAseq-targeted RNA Inflammation and Immunity Transcriptome panel kit (Qiagen, Hilden, Germany). Samples with RIN > 8.5 were used in sequencing analysis. Briefly, 400 ng of RNA was treated with DNase I and reverse transcribed. Next, 20 ng of cDNA was used in the barcode assignment procedure, followed by magnetic bead purification. Barcoded cDNA was amplified during 8-cycle PCR and purified using magnetic beads. Next, 1st-stage barcoded PCR products were uniquely indexed during the 22-cycle 2nd-stage PCR step. Final PCR amplicons were purified using magnetic beads. NGS libraries were quantified using a Qubit™ High Sensitivity dsDNA Quantification Assay kit (Invitrogen™, Thermo Fisher Scientific, Bleiswijk, The Netherlands) on a Qubit 4.0 fluorometer (Invitrogen™, Thermo Fisher Scientific, Bleiswijk, The Netherlands). Size ranges of NGS libraries were determined using a High Sensitivity DNA 1000 kit (Agilent Technologies, Santa Clara, CA, USA) on the Agilent 2100 device. Libraries were appropriately denatured and diluted according to the NextSeq library denaturation and dilution guide. A sequencing run was performed on the Illumina NextSeq 550 sequencer (Illumina, San Diego, CA, USA) using 150-cycle Illumina High Output Kit v2.5 (Illumina, San Diego, CA, USA).

2.8. Statistical Analysis

Statistical analyses and graphical representations were performed using GraphPad Prism 9 software (GraphPad Software Inc., San Diego, CA, USA). The animal body weight, thymus weight data, thymic cortex/medulla areas ratio, and HC count are expressed as mean \pm SD values. The ratio of the areas of the cortex and medulla in each individual of the group was calculated, and the mean value was obtained. The normality assumption of the thymus based on research and *Slc5a8* expression data distribution were evaluated and verified using the Shapiro–Wilk test. Quantitative differences between the two groups were evaluated using the Mann–Whitney *U* test. Results with a value of $p < 0.05$ were considered statistically significant.

2.9. Bioinformatic Analysis

The quality of the data was assessed using MultiQC v1.13 [57]. Adapter sequences with 3' nucleotides and sequences shorter than 15 nucleotides, as well as sequences with a quality score lower than 25, were removed using Cutadapt v1.9.1 [58]. The human genome (GRCh38.p13) was downloaded from the Ensembl database [59]. The remaining sequences were aligned to the human genome using the STAR 2.1.3 tool [60]. The gene expression matrix was obtained using FeatureCounts v3.15 [61]. Sequence expression was normalized using the upper quartile method, and genes with a total expression across samples less than 50 were removed. Differential gene expression analysis was performed using DESeq2 v3.15 [62], and *p*-values were adjusted using the Benjamin–Hochberg method. Enrichment analysis of biological pathways was conducted using the DAVID server [63,64].

Data from treated cells were compared with untreated thymocytes ($n = 6$). Gene expression data from treated and control conditions were normalized and logarithmically transformed. Enrichment analysis results from Gene Set Enrichment Analysis (GSEA) were analyzed using the Enrichplot v1.2 and ClusterProfiler v4.8.2 R packages [65]. GSEA was performed using predefined algorithms to calculate enrichment scores and *p*-values for each dominant pathway or gene set. Gene set annotations were obtained from the Gene Ontology (GO), KEGG, and Reactome databases. The impact of DCA–VPA treatment was

calculated by comparing gene expression in treated and control mouse cells. Significant changes in gene expression were determined when $p < 0.05$.

3. Results and Discussion

3.1. Effects of DCA–VPA Treatment on Body Weight, Thymus Structure, and Number of Hassall’s Corpuscles in the Medulla of the Thymus

The thymus is the central organ of the immune system, where T lymphocytes are formed, mature, and differentiate from thymocytes [66]. Under malnutrition or infection, mice show atrophy of the thymus, markedly reduced cortical tissue, a thymocyte count in the gland, and changes in chemokines and cytokines in the thymus tissue [53]. The mammalian thymus lobe structure is divided into the cortex and the medulla, with the cortex having a higher density of lymphocytes than the medulla. Immature CD4[−]CD8[−] (double-negative; DN) and CD4⁺CD8⁺ (double-positive; DP) thymocytes are located in the thymic cortex, whereas more mature CD4⁺CD8[−] or CD4[−]CD8⁺ single-positive thymocytes are located in the medulla [67]. It is, therefore, equally important in drug studies to determine the effect of the investigational medicine preparation on the weight of the animal and the weight and structural changes in the thymus.

This study found a significant increase in body weight over two weeks in the control animals ($n = 12$; 16.90 ± 2.33 g at the start and 20.68 ± 2.16 g at the end of the investigation; $p < 0.0006$) and the DCA–VPA-treated animal group ($n = 12$; 18.89 ± 1.30 g vs. 21.53 ± 1.33 g, respectively; $p < 0.0001$). DCA–VPA treatment did not affect body weight gain in the animals ($p > 0.05$). DCA–VPA treatment also did not affect thymus weight in mice (0.118 ± 0.011 g in the control and 0.118 ± 0.028 g in the treated group; $p > 0.05$). Previously, we reported that 4 weeks of monotherapy with DCA, at twice the dose of the DCA–VPA combination, caused a thymus weight decrease in DCA-treated gonad-intact male rats compared with their control, and no such impact was found in castrated DCA-treated males [54]. Also, VPA monotherapy at twice the dose of the DCA–VPA combination significantly reduced the thymus weight of castrated male Wistar rats after 4 weeks of treatment. However, it did not affect the thymus weight of intact males [68].

The thymic cortex/medulla ratio test can be used as an objective parameter to determine the effect of an investigational drug. Thymic atrophy and the associated decrease in the cortical/medulla ratio may be helpful as a quantitative indirect marker for screening histological examination [69]. The thymus contains a unique structure called Hassall’s corpuscles (HCs) found in the medulla. HCs appear as a collection of cells with a typical diameter of 20–100 μm [70]. The size of HCs correlates with the thymus size [71], making it difficult to detect in the mouse gland and for visualization requiring antigen-specific immunolabelling. Figure 1 shows immunohistochemical images of thymus specimens: histological specimens show the cortical and medullary areas and the HCs in the medulla.

Comparison of the thymus cortex and medulla histological structure of the control and the DCA–VPA-treated groups ($n = 6$ in each group) did not show a significant effect of 2 weeks of treatment. No DCA–VPA treatment effect was determined on the cortex-and-medulla ratio (3.30 ± 0.72 of control and 3.49 ± 1.25 of DCA–VPA-treated mice thymus; $p > 0.05$). The comparison of the number of HCs between the control group (9.70 ± 5.53 in mm^2) and the DCA–VPA-treated group (8.18 ± 2.76 in mm^2) revealed no significant difference ($p > 0.05$). It was reported that 4 weeks of treatment with high DCA doses caused a significant increase in the number of HCs in gonad-intact males but not in castrated rats [54].

The structure of HCs is the final stage of differentiation of the Aire⁺ lineage [72,73]. The size and number of HCs decrease with gland involution [74]. Human studies have shown that the AIRE gene is located on chromosome 21: the trisomy of chromosome 21 in patients (Down syndrome) results in a greater size and number of HCs in the thymus [75]. The formation of HCs is thought to be linked to an aging atrophy phenotype with reduced IFN α production, suggesting that the lack of an inflammatory signal leads to impaired thymocyte development [76]. Confirmation that medullary thymic epithelial cells (mTECs)

and HCs are involved in the induction of a pro-inflammatory microenvironment was obtained by studying Aire KO mice, which are depleted of post-Aire cells, and HCs are nearly missing in the Aire KO mouse [77] and have reduced expression of inflammatory mediators [76]. HCs may be necessary for the lymphoid tissue microenvironment's specific tonic inflammatory signaling. HCs express thymic stromal lymphopoietin, which can induce normal T cells to Treg [78,79]. The evidence of mTECs and HCs as inducers of tonic pro-inflammatory microenvironments in the thymus [80] highlights the importance of studying the effects of investigational drugs on the expression of genes involved in thymocytes in inflammation and the immune response.

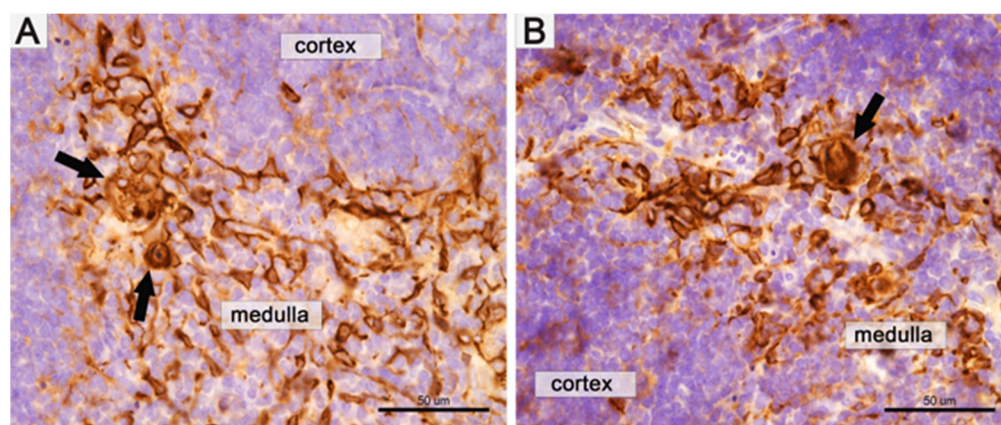


Figure 1. Immunohistochemical images of the Balb/c male mouse thymus. (A)—Thymus of the control group mouse (the cortex and medulla). (B)—Image of the DCA–VPA-treated mouse preparation. Hassall's corpuscles (arrows) in the medulla. Thymic epithelial cells and HCs are positive for high-molecular-weight cytokeratins (clone 34βE12). Scale bar of (A,B)—50 μm.

3.2. The Effect of DCA–VPA Treatment on Thymocytes' *Slc5a8* Gene Expression

Table 1 shows the effect of the DCA–VPA on *Slc5a8* RNR expression in the thymocytes of Balb/c male mice in vivo.

Table 1. *Slc5a8* expression in male mouse thymocytes of the studied groups.

Groups Studied	<i>n</i>	Ct Mean		$\Delta\text{Ct Mean} \pm \text{SEM}$	$\Delta\Delta\text{CT}$
		<i>Slc5a8</i>	<i>Gapdh</i>		
Control	6	34.77	19.49	15.27 ± 0.329	−1.63
DCA–VPA-treated	6	33.40	19.76	13.64 ± 0.351 ^a	

^a $p = 0.015$, compared with the control.

Two weeks of treatment with the combination of DCA 100 mg/kg per day and VPA 150 mg/kg per day results in a significant upregulation of *Slc5a8* by 2.1-fold in thymocytes of Balb/c male mice. Figure 2 shows the effect of DCA–VPA treatment on *Slc5a8* co-transporter gene expression in the thymocytes.

Compared to the control, the combination treatment resulted in a significant increase in *Slc5a8* expression in thymocytes; thus, the synergistic mechanism is manifested by VPA, improving the cellular transport of DCA and thus enhancing the pharmacological effects of DCA. Higher co-transporter expression may lead to better substrate accumulation in the cell. *Slc5a8* is a sodium- and chloride ion-dependent and sodium-linked monocarboxylate co-transporter that transports the dichloroacetate anion into cells [81,82]. Studies in male wild-type *c/ebpδ^{+/-}* and *c/ebpδ^{-/-}* mice indicate that *Slc5a8* has a physiological role in the transport of short-chain fatty acids as a substrate for the β-oxidation pathway in mitochondria into the cell. Upregulated *Slc5a8* is essential in regulating mice's cell metabolism and inflammation mechanisms [83]. The importance of *Slc5a8* for immune homeostasis

and inhibition of inflammation is highlighted. Short-chain fatty acids transported to immune cells via Slc5a8 alter HDAC activity and have immunomodulatory effects, such as blocking the development of dendritic cells, releasing cytokines, and inducing T-cell apoptosis [81,83]. *Slc5a8* expression can be upregulated by DNA demethylation. VPA can induce the effect on *Slc5c8* gene expression upregulation via DNA demethylation in cancer cells [81,84].

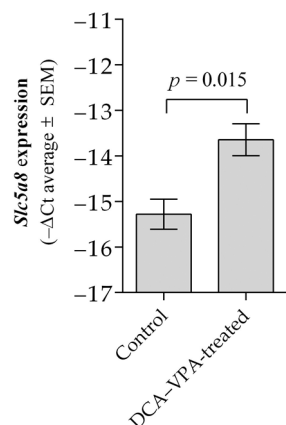


Figure 2. Slc5a8 co-transporter gene expression changes after treatment with DCA-VPA.

3.3. The Effect of DCA-VPA on Related Inflammation and Immune Response Genes' Expression in Mice Thymocytes

It was reported that the human and mouse thymus is a distinct organ that produces pro-inflammatory mediators even under physiological conditions [85,86]. Therefore, with its constant microenvironment tonic inflammation background, the thymus can be used as a model for studying the effects of investigational drugs that suppress inflammation and the immune response through changes in the expression of inflammation- and immune-response-related genes in thymocytes.

Table 2 shows the mean and log₂ data for the expression of genes related to inflammation and the immune response in thymocytes in the control and DCA-VPA-treated groups and the log₂ change comparing the control and treated groups. Genes with significantly increased expression after DCA-VPA treatment are shown in green, and genes with significantly decreased expression after treatment are shown in yellow.

Table 2. Expression of genes related to inflammation and immune response in male mice thymocytes in the control and DCA-VPA-treated groups.

Gene	Log ₂ Fold Change	Gene Expression (Average)		Gene Expression (Log ₂)		p Value
		Treated	Control	Treated	Control	
<i>Bmp4</i>	0.878	108.197	58.504	6.758	5.870	0.036
<i>Bmp7</i>	0.661	212.423	134.572	7.731	7.072	0.029
<i>C3</i>	0.598	7367.336	4867.781	12.847	12.249	0.024
<i>Ccl19</i>	0.667	260.248	163.851	8.024	7.356	0.035
<i>Ccl25</i>	1.427	28,348.999	10,540.968	14.791	13.364	8.92×10^{-7}
<i>Ciita</i>	0.828	1867.537	1052.728	10.867	10.040	2.27×10^{-5}
<i>Cmklr1</i>	0.848	653.655	363.705	9.352	8.507	0.0001
<i>Cx3cl1</i>	1.156	708.182	317.965	9.468	8.313	0.0020
<i>Cxcl11</i>	0.883	1184.140	641.946	10.210	9.326	0.0143
<i>Cxcl12</i>	1.593	10,218.765	3386.550	13.319	11.726	3.87×10^{-7}
<i>Cxcl13</i>	1.242	1620.704	685.156	10.662	9.420	0.0014
<i>Il2</i>	0.920	63.683	33.400	5.993	5.062	0.033
<i>Il7</i>	0.966	2624.135	1343.731	11.358	10.392	0.0005
<i>Il21</i>	0.912	30.857	16.548	4.948	4.049	0.038
<i>Il23a</i>	0.976	118.014	59.799	6.883	5.902	0.029

Table 2. Cont.

Gene	Log ₂ Fold Change	Gene Expression (Average)		Gene Expression (Log ₂)		p Value
		Treated	Control	Treated	Control	
<i>Il27</i>	0.727	82.518	49.879	6.367	5.640	0.039
<i>Il33</i>	0.639	645.356	414.507	9.334	8.695	0.027
<i>Kitl</i>	1.077	566.866	268.273	9.147	8.068	0.0005
<i>Nos2</i>	1.337	136.272	54.373	7.090	5.765	0.0043
<i>Pparg</i>	1.246	879.010	370.480	9.780	8.533	0.013
<i>Ccl2</i>	−1.081	949.215	2007.774	9.891	10.971	0.012
<i>Ccl3</i>	−0.844	1822.248	3270.595	10.832	11.675	0.009
<i>Ccr5</i>	−1.041	552.400	1135.583	9.110	10.149	2.65×10^{-5}
<i>Cdkn1a</i>	−0.639	2633.161	4101.501	11.363	12.002	0.017
<i>Cebpb</i>	−0.746	12,316.158	20,655.910	13.588	14.334	0.005
<i>Csf3</i>	−2.767	14.791	98.700	3.887	6.625	8.20×10^{-6}
<i>Cxcl1</i>	−1.694	1174.780	3801.410	10.198	11.892	0.007
<i>Cxcl2</i>	−1.723	719.590	2373.510	9.491	11.213	3.14×10^{-5}
<i>Cxcl3</i>	−1.073	150.984	317.559	7.238	8.311	0.0028
<i>Il1rl1</i>	−1.021	79.044	159.541	6.305	7.318	0.0003
<i>Il6</i>	−2.238	678.207	3198.631	9.406	11.643	0.0005
<i>Il17f</i>	−1.119	49.106	106.128	5.618	6.730	0.0017
<i>Il18r1</i>	−0.608	1246.327	1898.444	10.283	10.891	0.01
<i>Rel</i>	−0.691	3225.337	5204.208	11.655	12.345	0.0003
<i>Ptgs2</i>	−0.611	878.529	1340.712	9.779	10.389	0.005
<i>Spp1</i>	−1.142	343.025	757.012	8.422	9.564	0.0004
<i>Tnfsf11</i>	−0.669	2933.322	4664.196	11.518	12.187	0.042
<i>Thbs1</i>	−1.616	309.798	948.572	8.275	9.890	0.0008
<i>Vegfa</i>	−0.753	3633.337	6122.907	11.827	12.580	0.007

When comparing the changes in genes related to inflammation and the immune response in control and treated male mice, 19 genes were significantly decreased in the thymocytes of the mice treated for two weeks with the DCA–VPA combination, i.e., *Ccl2*, *Ccl3*, *Ccr5*, *Cdkn1a*, *Cebpb*, *Csf3*, *Cxcl1*, *Cxcl2*, *Cxcl3*, *Il17f*, *Il18r1*, *Il1rl1*, *Il6*, *Ptgs2*, *Rel*, *Spp1*, *Thbs1*, *Tnfsf11*, and *Vegfa*, and there was a significant increase in the expression of 20 genes, i.e., *Bmp4*, *Bmp7*, *C3*, *Ccl19*, *Ccl25*, *Ciita*, *Cmklr1*, *Cx3cl1*, *Cxcl11*, *Cxcl12*, *Cxcl13*, *Il2*, *Il7*, *Il21*, *Il23a*, *Il27*, *Il33*, *Kitl*, *Nos2*, and *Pparg*. Figure 3 shows data on the effect of DCA–VPA treatment on the expression of genes significantly downregulated or upregulated in male mice thymocytes.

3.3.1. A Possible DCA–VPA Treatment Effect on Thymus Function

In the context of the development of new drugs that inhibit inflammation and the immune response, it is essential to identify their effects on the integrated function of the thymus, possible adverse effects on T-lymphocyte lymphopoiesis, and changes in the signals to the T-cell progenitors from the thymus.

Compared to controls, a two-week treatment of mice with DCA–VPA increased the expression of *Cxcl12*, *Il2*, and *Il7* in thymus cells and inhibited the expression of *Il6* and *Ccl25* (Figure 3). *Cxcl12* promotes cell proliferation and differentiation to DN4 and the DP stage [87]. *Cxcl12* is linked to DP cell migration and its receptor *Cxcr4* is highly expressed in this cell population [88]. *Cxcl12* binds to the *Cxcr4* receptor and attracts immature $CD4^-CD8^-$ and $CD4^+CD8^+$ cells, and all thymocyte subsets are responsive to *Ccl25*, while its *Ccr9* receptor is expressed in all stages of thymocyte differentiation in mice (five-fold). Since *Ccr9* is reduced in mature thymocytes and *Ccl25* sensitivity is lost just before thymocyte emigration, the *Ccl25/Ccr9* interaction appears vital in thymic cell retention [89]. Thus, the effect of DCA–VPA, which may be related to the release of T cells from the thymus, cannot be excluded. Thymocyte differentiation and the release of mature T lymphocytes depend on the tissue microenvironmental cytokines *Il2*, *Il6*, and

Il7 [66]. Il2 is a pro-inflammatory cytokine, and its increase due to DCA–VPA exposure could be considered a positive effect, as it has been reported that thymocytes from acutely infected mice with *T. cruzi* have a reduced response to mitogens due to reduced secretion of Il2 [90]. Il6 can promote mitogen-induced thymocyte proliferation, associated with its anti-apoptotic function; Il6 induces CD8⁺ T-cell proliferation in synergy with Il7 [91]. In mice, Il7 production is associated with improved thymic cell health and functionality: Il7 is involved in normal T-lymphocyte development, stimulates survival and expansion of immature thymocytes, and increases thymocyte numbers [92,93].

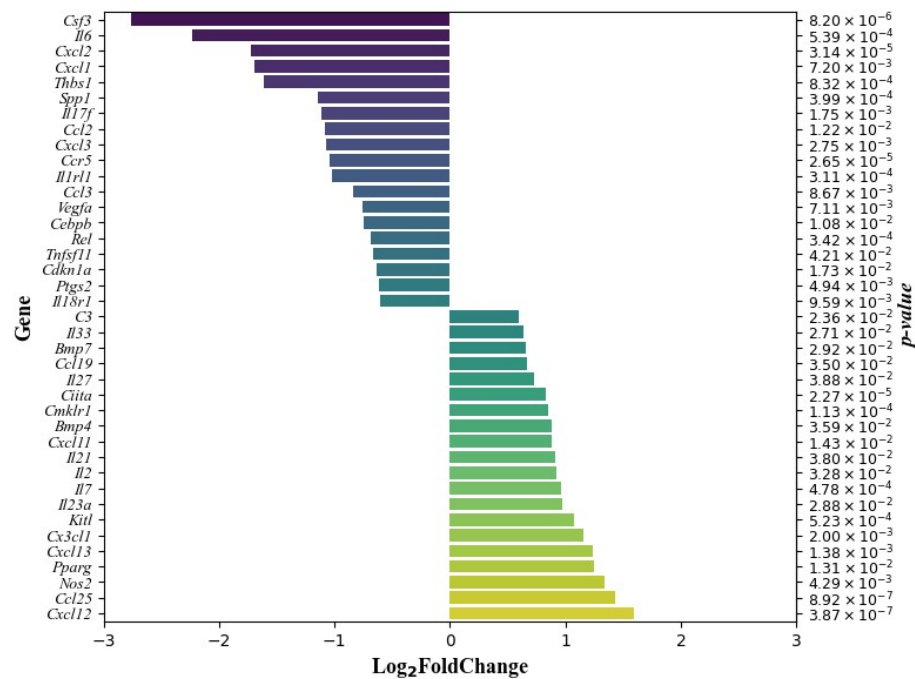


Figure 3. Genes whose expression in mouse thymocytes was significantly changed by DCA–VPA treatment. The data are expressed as Log₂ fold change—genes with reduced expression are shown in descending order of repression, and genes with upregulated gene expression are shown in ascending order of repression.

3.3.2. Effects of DCA–VPA Treatment on Cytokine Activity Pathway, Inflammatory Response Pathway, and Il17 Signaling Pathway Genes in Male Balb/c Mice Thymocytes

The differently expressed genes between control and DCA–VPA-treated thymic cells are enriched in the cytokine activity, inflammatory response pathway, and Il17 signaling pathway, as demonstrated by GO and KEGG analysis. Table 3 shows the genes involved in the biological pathways of cytokine activity, inflammatory response, and Il17 signaling in thymocytes, and the effects of DCA–VPA treatment on genes.

Table 3. Effects of DCA–VPA treatment on male mouse thymocyte genes for cytokine activity, inflammatory response, and Il17 signaling pathways.

Category and Term of Pathway	Count of Genes	p Value	Gene Expression	Fold Enrichment	p Value by Benjamini–Hochberg Method
GOTERM_MF_DIRECT—GO:0005125~cytokine activity	25	7.15 × 10 ^{−30}	Decreased: <i>Ccl2</i> , <i>Ccl3</i> , <i>Csrf3</i> , <i>Cxcl1</i> , <i>Cxcl2</i> , <i>Cxcl3</i> , <i>Il17f</i> , <i>Il6</i> , <i>Spp1</i> , <i>Tnfsf11</i> , <i>Vegfa</i> Increased: <i>Bmp4</i> , <i>Bmp7</i> , <i>Ccl19</i> , <i>Ccl25</i> , <i>Cx3cl1</i> , <i>Cxcl12</i> , <i>Cxcl13</i> , <i>Il2</i> , <i>Il7</i> , <i>Il21</i> , <i>Il23a</i> , <i>Il27</i> , <i>Il33</i> , <i>Kitl</i>	31.10	1.75 × 10 ^{−27}

Table 3. Cont.

Category and Term of Pathway	Count of Genes	<i>p</i> Value	Gene Expression	Fold Enrichment	<i>p</i> Value by Benjamini–Hochberg Method
GOTERM_BP_DIRECT—GO:0006954~inflammatory response	25	2.01×10^{-27}	Decreased: <i>Ccl2</i> , <i>Ccl3</i> , <i>Ccr5</i> , <i>Cxcl1</i> , <i>Cxcl2</i> , <i>Cxcl3</i> , <i>Il1rl1</i> , <i>Il6</i> , <i>Il17f</i> , <i>Il18r1</i> , <i>Ptgs2</i> , <i>Rel</i> , <i>Thbs1</i> Increased: <i>C3</i> , <i>Ccl19</i> , <i>Ccl25</i> , <i>Ciita</i> , <i>Cmklr1</i> , <i>Cx3cl1</i> , <i>Cxcl11</i> , <i>Cxcl13</i> , <i>Il23a</i> , <i>Il27</i> , <i>Nos2</i> , <i>Pparg</i>	20.20	2.81×10^{-24}
KEGG_PATHWAY—hsa04657: IL-17 signaling pathway	9	7.94×10^{-8}	Decreased: <i>Ccl2</i> , <i>Cebpb</i> , <i>Csf3</i> , <i>Cxcl1</i> , <i>Cxcl2</i> , <i>Cxcl3</i> , <i>Il6</i> , <i>Il17f</i> , <i>Ptgs2</i>	15.40	2.16×10^{-6}

DCA–VPA Effects on the Cytokine Activity Pathway

Sequencing analysis showed that the treatment of male mice with DCA–VPA had a significant effect on 25 genes of the cytokine activation pathway: 11 genes' expression was significantly decreased, and 14 genes' expression was significantly increased by treatment (Figure 2, Tables 2 and 3). Compared to the control, in the DCA–VPA-treated thymocytes group, decreased *Ccl2*, *Ccl3*, *Csf3*, *Cxcl1*, *Cxcl2*, *Cxcl3*, *Il17f*, *Il6*, *Spp1*, *Tnfsf11*, and *Vegfa* gene expression was found. Such test drug effects on inflammation and immune-response-related genes could be seen as suppressing inflammation and the immune response. *Ccl2* and *Ccl3* chemokines are classified as pro-inflammatory: *Ccl2* stimulates chemotaxis of monocytes and a few cellular events associated with chemotaxis: *Ccl3* function, macrophage–NK migration, and T-cell/DC interaction [94]. *Cxcl1*, *Cxcl2*, and *Cxcl3* chemokines' function is neutrophil trafficking [94]. *Cx3cl1* is expressed mainly in immune cells, including monocytes and T cells, and deficiency of *Cx3cr1* promotes pro-inflammatory cytokine production in macrophages and T cells [95]. *Cx3cl1* acts via the *Cx3cl1/Cx3cr1* axis: the chemokine receptor *Cx3cr1* is a known marker of anti-inflammatory monocytes, providing a pro-survival signal to anti-inflammatory monocytes; it also presents in NK cells and T cells, where it mediates proliferation, migration, and adhesion [94,96]. Helper T cells (Th17) are potent inducers of tissue inflammation by releasing *Il17f* [97]. *Il6* plays an important role during the early immune response to infection, causing B lymphocytes to differentiate into mature, immunoglobulin-secreting plasma B cells; signaling also initiates T-cell activation, growth, and differentiation [98]. *Spp1* at the cellular level is expressed in macrophages, dendritic cells, lymphoid cells, and mononuclear cells of the immune system [99]: severe COVID-19 disease is associated with macrophage SPP1 production, and SPP1 leads to the strong inflammatory response characteristic of severe COVID-19 disease [100]. Reduced gene expression of *Tnfsf11* in thymocytes is associated with the differentiation of mature thymocytes into Tregs and cell release [101]; Tregs suppress the immune response, maintain homeostasis, and may inhibit T-cell proliferation and cytokine production [102]. *Vegf* and its receptor's upregulation is linked to the pathophysiology of several human viral diseases [103].

The effect of DCA–VPA on the reduction in *Csf3* expression needs to be addressed separately. *Csf3* (granulocyte colony-stimulating factor; G-CSF) is an essential cell growth factor that supports neutrophil progenitor cell proliferation, survival, and differentiation and is a potent immune regulator of T cells [104]. G-CSF is released from lung cells in response to the pro-inflammatory cytokines TNF- α and *Il1 β* [105]. G-CSF receptor (G-CSFR) blockade reduces neutrophil infiltration and neutrophil-mediated inflammation in mouse models of infection and asthma [106,107]. The blockade of G-CSF or its receptor G-CSFR could be a treatment strategy for such patients. A case report describing the onset of ARDS

in five patients in whom G-CSF was administered in combination with chemotherapy or hematopoietic cell transplantation has been published [108]. G-CSF administration may worsen lung function, especially in cytokine release syndrome, sepsis, or ARDS, which are also critical features of COVID-19 disease [105].

Compared to the control, in the DCA–VPA-treated thymocytes group, increased *Bmp4*, *Bmp7*, *Ccl19*, *Ccl25*, *Cx3cl1*, *Cxcl12*, *Cxcl13*, *Il2*, *Il7*, *Il21*, *Il23a*, *Il27*, *Il33*, and *Kitl* gene expression was found in mice thymocytes. *Bmp4* molecules were found to act as a host response against SARS-CoV-2 [109]. Studies have shown that *Bmp7* is an anti-inflammatory factor that downregulates basal and TNF α -stimulated production of the pro-inflammatory cytokines *Il6*, *Il8*, and *Il1 β* , along with the chemokine *Ccl2*, and induces M2 macrophage differentiation [110,111]. *Ccl19* and *Ccl25* chemokines' function is as homeostatic thymocyte migration induction: *Ccl19* is responsible for T-cell and dendritic cell homing to lymph node, and *Ccl25* is responsible for T-cell homing to the gut [94]. The *Cxcl12* chemokine is responsible for bone marrow homing, while *Cxcl13* is responsible for B-cell positioning in lymph nodes [94]. Thus, the DCA–VPA treatment is related to an anti-inflammatory effect. *Il2* and *Il21* have specific functions during T-cell differentiation and homeostasis [112], while *Th17* are potent inducers of tissue inflammation through the release of *Il21* [97]. However, our study shows that DCA–VPA inhibits the *Th17* pathway. *Il7* regulates immature and mature T-lymphocyte homeostasis [113]. *Il23a* plays a role in inflammation, the immune response, and cell differentiation and survival [98]. *Il27* is involved in helper T-cell differentiation [114]. *Il33* is pro-inflammatory [98]. *Kitl* is a thymopoietic molecule [115]. In *Il33* knockout mice, it was discovered that nuclear *Il33* is associated with wound healing, as mice without the protein healed significantly slower than mice with the *Il33* protein [116]. The functions of the above-mentioned related cytokine activity pathway genes suggest that DCA–VPA has anti-inflammatory and immunosuppressive properties by inhibiting the cytokine activity pathway.

DCA–VPA Effects on the Inflammatory Response Pathway

The DCA–VPA treatment significantly affected 25 genes of the inflammatory response pathway: 13 genes overlap with the cytokine response pathway, 7 genes' expression is decreased (*Ccl2*, *Ccl3*, *Cxcl1*, *Cxcl2*, *Cxcl3*, *Il6*, *Il17f*), and 7 are upregulated (*Ccl19*, *Ccl25*, *Cx3cl1*, *Cxcl11*, *Cxcl13*, *Il23a*, *Il27*). Treatment with the investigational drug had an anti-inflammatory effect by significantly suppressing *Ccr5*, *Il1rl*, *Ptgs2*, *Rel*, and *Thbs1* expression. *Ccr5* (chemokine receptor 5) is a common receptor for the chemotactic mediators *Ccl3*, *Ccl4*, and *Ccl5*. *Ccr5* is expressed in many inflammatory cell lines, including T cells. The expression of *Ccr5* is upregulated in models of inflammation, and *Ccr5* antagonism may be a promising therapeutic strategy [117]. As indicated above, DCA–VPA increased *Il33* expression in Balb/c thymocytes but inhibited *Il1rl* (*St2*) receptor expression. *Il33* targets are type 1 and type 2 immune cells. The *Il1rl1* receptor is essential for the mechanisms underlying *Il33* inflammation. *Il33* is released after cell damage or tissue injury and activates signaling pathways in cells harboring the *Il1rl1* receptor. Thus, DCA–VPA could indirectly inhibit *Il33*-induced mechanisms by inhibiting *Il1rl1* gene expression. Mouse models support an essential *Il33*/*St2* signaling role in allergic inflammatory mechanisms (in the nasopharynx, lung, and skin tissues). *Il33*/*St2* is also important for non-allergic inflammatory pathways [118]. *Ptgs2* (prostaglandin-endoperoxide synthase 2; *Cox2*) is a pro-inflammatory cyclooxygenase whose activity increases during inflammation. *Cox2* is important for the production of pro-inflammatory eicosanoids. *Cox2* gene expression is induced by the cytokines *Il1 β* and TNF α [119]. *Rel* is a member of the NF- κ B/*Rel* family of transcription factors restricted by hemopoietic cells and important for T-lymphocyte function. *Rel*^{-/-} mice had a significantly reduced T-cell proliferative response to the virus and attenuated local and systemic influenza virus-specific antibody responses, with normal levels of virus-specific cytotoxic T lymphocytes, which were able to clear the virus from the mouse lungs [120]. *Thbs1* (thrombospondin 1) is released and increased during the acute

phase of inflammation and plays a synergistic role in the inflammatory process; *Thbs1* is a pro-inflammatory factor [120], which was increased among COVID-19 patients [121].

The upregulation effect of DCA–VPA treatment on inflammatory response pathway genes was found to overlap seven genes with the cytokine response pathway (*Ccl19*, *Ccl25*, *Cx3cl1*, *Cxcl11*, *Cxcl13*, *Il23a*, *Il27*). Additionally, the expression of five genes (*C3*, *Ciita*, *Cmklr1*, *Nos2*, *Pparg*) was found to be significantly increased by the treatment with DCA–VPA in thymocytes, which is also linked to the anti-inflammatory effects of test preparation. C3 protein is mainly located in thymic corpuscles, which may be involved in immune regulation [122]. C3 plays a crucial role in enhancing the T-cell response to bacterial infection by promoting the proliferation of antigen-exposed CD8 T cells [123]. Studies in mice show that C3 produced by the liver and lungs ensures the host's response to infection by stimulating immune resistance. C3 alleviates severe bacterial pneumonia: intracellular complement protein modulates cell survival and provides a putative mechanism by which lung-derived C3 protects from tissue damage induced by pneumonia [124]. *Ciita* is a key transactivator of major histocompatibility complex II expression and controls antigen presentation followed by T-cell activation [125]. The epigenetic regulation of *Ciita* by VPA is the suspected cause of the increased expression of *Ciita* in thymocytes due to demethylation after therapy with DCA–VPA. If this is the case, such an effect may be beneficial for cancer therapy, as epigenetic inhibition of *Ciita* in tumor cells may prevent the immune system from recognizing the tumor antigen and, thus, the anti-tumor immune response [126].

The significance of *Cmklr1* (chemokine-like receptor-1) is not fully understood [127,128]. *Cmklr1* deficiency reduces leukocyte recruitment to inflammation-damaged lungs [127]. On the other hand, activation of *Cmklr1* in a murine model of virus-induced pneumonia improved viral clearance and antiviral antibody production, reduced the expression of pro-inflammatory mediators, reduced complications, and improved mouse survival [129,130]. While clinical data are still lacking, preclinical data suggest that *Cmklr1* may be a lung inflammation biomarker in pneumonia patients [128]. The enzyme NOS2 (nitric oxide synthase 2) and reactive oxygen species (ROS) are players in inflammatory and immune responses. However, the functional significance of the link between NOS2 and ROS during infection remains unclear [131]. It cannot be excluded that the possible increase in NOS2 expression may be due to the generation of ROS induced by DCA and VPA [132,133]. Peroxisome proliferator-activated receptor- γ (*Pparg*) is involved in anti-inflammatory processes through immune cells and is in anti-inflammatory macrophages [134].

DCA–VPA Effects on the Il17 Signaling Pathway

DCA–VPA treatment reduced the expression of *Ccl2*, *Cebpb*, *Csf3*, *Cxcl1*, *Cxcl2*, *Cxcl3*, *Il6*, *Il17f*, and *Ptgs2* genes, which are involved in the Il17 signaling in the thymocytes of male Balb/c mice. These genes are also involved in cytokine activity and inflammatory response pathways (Table 2). Il17 plays a key role in the cytokine storm, in ARDS, and is associated with alveolar inflammation and poor prognosis [135]. In mouse models, direct blockade of Il17 reduced lung injury [136]. In severe cases of COVID-19, elevated levels of Il17 signaling pathway pro-inflammatory chemokines and cytokines are directly correlated with increased severity of lung injury and prognosis [137].

Inflammation is a defensive cellular response to pathogens, infection, or tissue damage. It coordinates the interactions between different immune cells, a complex chain of molecular signaling mechanisms, the release of inflammatory mediators (chemokines, cytokines, etc.), and their effects on tissues. The novelty of this preclinical study is that DCA–VPA treatment suppresses the inflammatory response in thymocytes. This finding is consistent with previous studies showing the anti-inflammatory properties of both DCA and VPA in monotherapy. The synergism between DCA and VPA in activating DCA transport into the cell via *Slc5a8* allows a reduction in the DCA dose.

A limitation of this study could be that while the thymus cell suspension used was composed of an absolute majority of T cells, a minority of other microenvironmental cells, such as thymic epithelial cells, dendritic cells, macrophages, and fibroblasts were

not separated [105], which may have influenced the gene expression data to some extent. Also, for synergism, an additional justification, besides the effect of the combination on *Slc5a8*, would be a comparison with an untreated control, monotherapy, and treatment with combination. Another limitation of the study is that only male Balb/c mice were tested, so the results presented may not be consistent with other populations and do not reveal sex differences as they were not compared with similar data from female mice. However, the preclinical study data obtained are undoubtedly relevant for evaluating the anti-inflammatory effects of preparation, which are essential for further studies on the pharmacological efficacy of the DCA–VPA.

4. Conclusions

The treatment with the DCA–VPA combination did not affect the weight of the Balb/c male mice's thymus and its structure. DCA–VPA significantly increased *Slc5A8* gene expression in thymocytes, suggesting that VPA as an epigenetic demethylating agent may improve the intracellular delivery of DCA. Thymocytes are enriched in the cytokine activity pathway, inflammatory response pathway, and *Il17* signaling pathway. DCA–VPA exhibits anti-inflammatory effects by inhibiting the inflammatory mechanisms of the pathways mentioned above by suppressing the expression of pro-inflammatory genes and activation of anti-inflammatory chemokines' and cytokines' gene expression in the thymocytes of male mice.

5. Patent

Medicinal product DCA–VPA is patented as a new medicinal product for the treatment of viral and bacterial infections (national patent application no. LT2023 532; 22 August 2023).

Author Contributions: Conceptualization, V.L. and D.S.; formal analysis, I.B., L.Š. and J.P.; funding acquisition, V.L. and D.S.; investigation, E.K., D.G., L.K., I.B., L.Š. and J.P.; methodology, V.L., D.S., D.G., L.K. and I.B.; project administration, V.L. and D.S.; resources, V.L., I.B. and D.G.; software, D.G. and L.K.; supervision, V.L.; validation, D.G., L.K. and I.B.; visualization I.B., L.K. and D.G.; writing—original draft, D.S. and V.L.; writing—review and editing, all authors. All authors have read and agreed to the published version of the manuscript.

Funding: This project received funding from European Regional Development Fund (project no. 13.1.1-LMT-L-718-05-0030) under a grant agreement with the Research Council of Lithuania (LMTLT). It was funded as a European Union measure in response to the COVID-19 pandemic.

Institutional Review Board Statement: The study was approved by the State Food and Veterinary Service of Lithuania (No. G2-198 of 16 March 2022).

Informed Consent Statement: Not applicable.

Data Availability Statement: The data presented in this study are available on request from the corresponding author.

Conflicts of Interest: The authors declare no conflict of interest.

References

1. Fleischmann, C.; Scherag, A.; Adhikari, N.K.J.; Hartog, C.S.; Tsaganos, T.; Schlattmann, P.; Angus, D.C.; Reinhart, K. Assessment of Global Incidence and Mortality of Hospital-Treated Sepsis Current Estimates and Limitations. *Am. J. Respir. Crit. Care Med.* **2016**, *193*, 259–272. [[CrossRef](#)] [[PubMed](#)]
2. Vincent, J.L.; Bakker, J. Blood Lactate Levels in Sepsis: In 8 Questions. *Curr. Opin. Crit. Care* **2021**, *27*, 298–302. [[CrossRef](#)] [[PubMed](#)]
3. Langley, R.J.; Tsalik, E.L.; Van Velkinburgh, J.C.; Glickman, S.W.; Rice, B.J.; Wang, C.; Chen, B.; Carin, L.; Suarez, A.; Mohney, R.P.; et al. Sepsis: An Integrated Clinico-Metabolomic Model Improves Prediction of Death in Sepsis. *Sci. Transl. Med.* **2013**, *5*, 195ra95. [[CrossRef](#)] [[PubMed](#)]
4. Kotas, M.E.; Medzhitov, R. Homeostasis, Inflammation, and Disease Susceptibility. *Cell* **2015**, *160*, 816–827. [[CrossRef](#)] [[PubMed](#)]
5. Soares, M.P.; Teixeira, L.; Moita, L.F. Disease Tolerance and Immunity in Host Protection against Infection. *Nat. Rev. Immunol.* **2017**, *17*, 83–96. [[CrossRef](#)] [[PubMed](#)]

6. Shoraka, S.; Samarasinghe, A.E.; Ghaemi, A.; Mohebbi, S.R. Host Mitochondria: More than an Organelle in SARS-CoV-2 Infection. *Front. Cell. Infect. Microbiol.* **2023**, *13*, 1228275. [[CrossRef](#)] [[PubMed](#)]
7. Stakišaitis, D.; Kapočius, L.; Valančiūte, A.; Balnyte, I.; Tamošuitis, T.; Vaitkevičius, A.; Sužiedelis, K.; Urbonienė, D.; Tatarūnas, V.; Urbonienė, E.; et al. SARS-CoV-2 Infection, Sex-Related Differences, and a Possible Personalized Treatment Approach with Valproic Acid: A Review. *Biomedicines* **2022**, *10*, 962. [[CrossRef](#)]
8. Mainali, R.; Zabalawi, M.; Long, D.; Buechler, N.; Quillen, E.; Key, C.C.; Zhu, X.; Parks, J.S.; Furdai, C.; Stacpoole, P.W.; et al. Dichloroacetate Reverses Sepsis-Induced Hepatic Metabolic Dysfunction. *eLife* **2021**, *10*, e64611. [[CrossRef](#)]
9. Patel, M.S.; Nemeria, N.S.; Furey, W.; Jordan, F. The Pyruvate Dehydrogenase Complexes: Structure-Based Function and Regulation. *J. Biol. Chem.* **2014**, *289*, 16615–16623. [[CrossRef](#)]
10. James, M.O.; Jahn, S.C.; Zhong, G.; Smeltz, M.G.; Hu, Z.; Stacpoole, P.W. Therapeutic Applications of Dichloroacetate and the Role of Glutathione Transferase Zeta-1. *Pharmacol. Ther.* **2017**, *170*, 166–180. [[CrossRef](#)]
11. El Sayed, S.M.; Baghdadi, H.; Ahmed, N.S.; Almaramhy, H.H.; Mahmoud, A.A.A.; El-Sawy, S.A.; Ayat, M.; Elshazley, M.; Abdel-Aziz, W.; Abdel-Latif, H.M.; et al. Dichloroacetate Is an Antimetabolite That Antagonizes Acetate and Deprives Cancer Cells from Its Benefits: A Novel Evidence-Based Medical Hypothesis. *Med. Hypotheses* **2019**, *122*, 206–209. [[CrossRef](#)]
12. Zeng, Z.; Huang, Q.; Mao, L.; Wu, J.; An, S.; Chen, Z.; Zhang, W. The Pyruvate Dehydrogenase Complex in Sepsis: Metabolic Regulation and Targeted Therapy. *Front. Nutr.* **2021**, *8*, 783164. [[CrossRef](#)] [[PubMed](#)]
13. Park, S.; Jeon, J.H.; Min, B.K.; Ha, C.M.; Thoudam, T.; Park, B.Y.; Lee, I.K. Role of the Pyruvate Dehydrogenase Complex in Metabolic Remodeling: Differential Pyruvate Dehydrogenase Complex Functions in Metabolism. *Diabetes Metab. J.* **2018**, *42*, 270–281. [[CrossRef](#)] [[PubMed](#)]
14. McCall, C.E.; Zabalawi, M.; Liu, T.; Martin, A.; Long, D.L.; Buechler, N.L.; Arts, R.J.W.; Netea, M.; Yoza, B.K.; Stacpoole, P.W.; et al. Pyruvate Dehydrogenase Complex Stimulation Promotes Immunometabolic Homeostasis and Sepsis Survival. *JCI Insight* **2018**, *3*, e99292. [[CrossRef](#)] [[PubMed](#)]
15. Kelly, B.; O'Neill, L.A.J. Metabolic Reprogramming in Macrophages and Dendritic Cells in Innate Immunity. *Cell Res.* **2015**, *25*, 771–784. [[CrossRef](#)] [[PubMed](#)]
16. Eyenga, P.; Roussel, D.; Morel, J.; Rey, B.; Romestaing, C.; Gueguen-Chaignon, V.; Sheu, S.S.; Viale, J.P. Time Course of Liver Mitochondrial Function and Intrinsic Changes in Oxidative Phosphorylation in a Rat Model of Sepsis. *Intensive Care Med. Exp.* **2018**, *6*, 31. [[CrossRef](#)] [[PubMed](#)]
17. Nuzzo, E.; Berg, K.M.; Andersen, L.W.; Balkema, J.; Montissol, S.; Cocchi, M.N.; Liu, X.; Donnino, M.W. Pyruvate Dehydrogenase Activity Is Decreased in the Peripheral Blood Mononuclear Cells of Patients with Sepsis: A Prospective Observational Trial. *Ann. Am. Thorac. Soc.* **2015**, *12*, 1662–1666. [[CrossRef](#)] [[PubMed](#)]
18. Yang, K.; Fan, M.; Wang, X.; Xu, J.; Wang, Y.; Tu, F.; Gill, P.S.; Ha, T.; Liu, L.; Williams, D.L.; et al. Lactate Promotes Macrophage HMGB1 Lactylation, Acetylation, and Exosomal Release in Polymicrobial Sepsis. *Cell Death Differ.* **2022**, *29*, 133–146. [[CrossRef](#)]
19. Alamdari, N.; Constantin-Teodosiu, D.; Murton, A.J.; Gardiner, S.M.; Bennett, T.; Layfield, R.; Greenhaff, P.L. Temporal Changes in the Involvement of Pyruvate Dehydrogenase Complex in Muscle Lactate Accumulation during Lipopolysaccharide Infusion in Rats. *J. Physiol.* **2008**, *586*, 1767–1775. [[CrossRef](#)]
20. Singer, P.M.; De Santis, V.; Vitale, D.; Jeffcoate, W. Multiorgan Failure Is an Adaptive, Endocrine-Mediated, Metabolic Response to Overwhelming Systemic Inflammation. *Lancet* **2004**, *364*, 545–548. [[CrossRef](#)]
21. Colegio, O.R.; Chu, N.Q.; Szabo, A.L.; Chu, T.; Rhebergen, A.M.; Jairam, V.; Cyrus, N.; Brokowski, C.E.; Eisenbarth, S.C.; Phillips, G.M.; et al. Functional Polarization of Tumour-Associated Macrophages by Tumour-Derived Lactic Acid. *Nature* **2014**, *513*, 559–563. [[CrossRef](#)] [[PubMed](#)]
22. Samuvel, D.J.; Sundararaj, K.P.; Nareika, A.; Lopes-Virella, M.F.; Huang, Y. Lactate Boosts TLR4 Signaling and NF-κB Pathway-Mediated Gene Transcription in Macrophages via Monocarboxylate Transporters and MD-2 Up-Regulation. *J. Immunol.* **2009**, *184*, 2476–2484. [[CrossRef](#)] [[PubMed](#)]
23. Liu, Z.; Meng, Z.; Li, Y.; Zhao, J.; Wu, S.; Gou, S.; Wu, H. Prognostic Accuracy of the Serum Lactate Level, the SOFA Score and the QSOFA Score for Mortality among Adults with Sepsis. *Scand. J. Trauma. Resusc. Emerg. Med.* **2019**, *27*, 51. [[CrossRef](#)]
24. Planche, T. Malaria and Fluids—Balancing Acts. *Trends Parasitol.* **2005**, *21*, 562–567. [[CrossRef](#)] [[PubMed](#)]
25. An, S.; Yao, Y.; Hu, H.; Wu, J.; Li, J.; Li, L.; Wu, J.; Sun, M.; Deng, Z.; Zhang, Y.; et al. PDHA1 Hyperacetylation-Mediated Lactate Overproduction Promotes Sepsis-Induced Acute Kidney Injury via Fis1 Lactylation. *Cell Death Dis.* **2023**, *14*, 457. [[CrossRef](#)] [[PubMed](#)]
26. Zemlin, A.E.; Sigwadhi, L.N.; Wiese, O.J.; Jalavu, T.P.; Chapanduka, Z.C.; Allwood, B.W.; Tamuzi, J.L.; Koegelenberg, C.F.; Irušen, E.M.; Lalla, U.; et al. The Association between Acid–base Status and Clinical Outcome in Critically Ill COVID-19 Patients Admitted to Intensive Care Unit with an Emphasis on High Anion Gap Metabolic Acidosis. *Ann. Clin. Biochem.* **2023**, *60*, 86–91. [[CrossRef](#)] [[PubMed](#)]
27. Zhu, X.; Long, D.; Zabalawi, M.; Ingram, B.; Yoza, B.K.; Stacpoole, P.W.; McCall, C.E. Stimulating Pyruvate Dehydrogenase Complex Reduces Itaconate Levels and Enhances TCA Cycle Anabolic Bioenergetics in Acutely Inflamed Monocytes. *J. Leukoc. Biol.* **2020**, *107*, 467–484. [[CrossRef](#)]
28. McCall, C.E.; Zhu, X.; Zabalawi, M.; Long, D.; Quinn, M.A.; Yoza, B.K.; Stacpoole, P.W.; Vachharajani, V. Sepsis, Pyruvate, and Mitochondria Energy Supply Chain Shortage. *J. Leukoc. Biol.* **2022**, *112*, 1509–1514. [[CrossRef](#)]

29. Perucca, E. Pharmacological and Therapeutic Properties of Valproate: A Summary after 35 Years of Clinical Experience. *CNS Drugs* **2002**, *16*, 695–714. [[CrossRef](#)]
30. Michaelis, M.; Doerr, H.; Cinatl, J., Jr. Valproic Acid as Anti-Cancer Drug. *Curr. Pharm. Des.* **2007**, *13*, 3378–3393. [[CrossRef](#)]
31. Andreu, S.; Ripa, I.; Bello-Morales, R.; López-Guerrero, J.A. Valproic Acid and Its Amidic Derivatives as New Antivirals against Alphaherpesviruses. *Viruses* **2020**, *12*, 1356. [[CrossRef](#)]
32. Phiel, C.J.; Zhang, F.; Huang, E.Y.; Guenther, M.G.; Lazar, M.A.; Klein, P.S. Histone Deacetylase Is a Direct Target of Valproic Acid, a Potent Anticonvulsant, Mood Stabilizer, and Teratogen. *J. Biol. Chem.* **2001**, *276*, 36734–36741. [[CrossRef](#)] [[PubMed](#)]
33. Adcock, I.M. HDAC Inhibitors as Anti-Inflammatory Agents. *Br. J. Pharmacol.* **2007**, *150*, 829–831. [[CrossRef](#)] [[PubMed](#)]
34. Van Beneden, K.; Geers, C.; Pauwels, M.; Mannaerts, I.; Verbeelen, D.; Van Grunsven, L.A.; Van Den Branden, C. Valproic Acid Attenuates Proteinuria and Kidney Injury. *J. Am. Soc. Nephrol.* **2011**, *22*, 1863–1875. [[CrossRef](#)] [[PubMed](#)]
35. Roda, M.A.; Sadik, M.; Gaggar, A.; Hardison, M.T.; Jablonsky, M.J.; Braber, S.; Blalock, J.E.; Redegeld, F.A.; Folkerts, G.; Jackson, P.L. Targeting Prolyl Endopeptidase with Valproic Acid as a Potential Modulator of Neutrophilic Inflammation. *PLoS ONE* **2014**, *9*, e97594.
36. Roger, T.; Lugrin, J.; Le Roy, D.; Goy, G.; Mombelli, M.; Koessler, T.; Ding, X.C.; Chanson, A.L.; Reymond, M.K.; Miconnet, I.; et al. Histone Deacetylase Inhibitors Impair Innate Immune Responses to Toll-like Receptor Agonists and to Infection. *Blood* **2011**, *117*, 1205–1217. [[CrossRef](#)] [[PubMed](#)]
37. Jin, H.; Guo, X. Valproic Acid Ameliorates Coxsackievirus-B3-Induced Viral Myocarditis by Modulating Th17/Treg Imbalance. *Virology* **2016**, *13*, 168. [[CrossRef](#)]
38. Ximenes, J.C.M.; De Oliveira Gonçalves, D.; Siqueira, R.M.P.; Neves, K.R.T.; Santos Cerqueira, G.; Correia, A.O.; Félix, F.H.C.; Leal, L.K.A.M.; De Castro Brito, G.A.; Da Graça Naffah-Mazzacorati, M.; et al. Valproic Acid: An Anticonvulsant Drug with Potent Antinociceptive and Anti-Inflammatory Properties. *Naunyn-Schmiedeberg's Arch. Pharmacol.* **2013**, *386*, 575–587. [[CrossRef](#)]
39. Shyer, J.A.; Flavell, R.A.; Bailis, W. Metabolic Signaling in T Cells. *Cell Res.* **2020**, *30*, 649–659. [[CrossRef](#)]
40. Sinclair, L.V.; Rolf, J.; Emslie, E.; Shi, Y.B.; Taylor, P.M.; Cantrell, D.A. Control of Amino-Acid Transport by Antigen Receptors Coordinates the Metabolic Reprogramming Essential for T Cell Differentiation. *Nat. Immunol.* **2013**, *14*, 500–508. [[CrossRef](#)]
41. Kidani, Y.; Elsaesser, H.; Hock, M.B.; Vergnes, L.; Williams, K.J.; Argus, J.P.; Marbois, B.N.; Komisopoulou, E.; Wilson, E.B.; Osborne, T.F.; et al. Sterol Regulatory Element-Binding Proteins Are Essential for the Metabolic Programming of Effector T Cells and Adaptive Immunity. *Nat. Immunol.* **2013**, *14*, 489–499. [[CrossRef](#)]
42. Codo, A.C.; Davanzo, G.G.; de Brito Monteiro, L.; de Souza, G.F.; Muraro, S.P.; Virgilio-da-Silva, J.V.; Prodonoff, J.S.; Carregari, V.C.; de Biagi Junior, C.A.O.; Crunfli, F.; et al. Erratum: Elevated Glucose Levels Favor SARS-CoV-2 Infection and Monocyte Response through a HIF-1 α /Glycolysis-Dependent Axis. *Cell Metab.* **2020**, *32*, 437–446. [[CrossRef](#)] [[PubMed](#)]
43. Luan, Y.; Luan, Y.; He, H.; Jue, B.; Yang, Y.; Qin, B.; Ren, K. Glucose Metabolism Disorder: A Potential Accomplice of SARS-CoV-2. *Int. J. Obes.* **2023**, *47*, 893–902. [[CrossRef](#)] [[PubMed](#)]
44. Khan, S.; Jena, G. Valproic Acid Improves Glucose Homeostasis by Increasing Beta-Cell Proliferation, Function, and Reducing Its Apoptosis through HDAC Inhibition in Juvenile Diabetic Rat. *J. Biochem. Mol. Toxicol.* **2016**, *30*, 438–446. [[CrossRef](#)] [[PubMed](#)]
45. Rakitin, A.; Köks, S.; Haldre, S. Valproate Modulates Glucose Metabolism in Patients with Epilepsy after First Exposure. *Epilepsia* **2015**, *56*, 172–175. [[CrossRef](#)] [[PubMed](#)]
46. Schoenmann, N.; Tannenbaum, N.; Hodgeman, R.M.; Raju, R.P. Regulating Mitochondrial Metabolism by Targeting Pyruvate Dehydrogenase with Dichloroacetate, a Metabolic Messenger. *Biochim. Biophys. Acta-Mol. Basis Dis.* **2023**, *1869*, 166769. [[CrossRef](#)] [[PubMed](#)]
47. Milutinovic, S.; Detich, N.; Szyf, M. Valproate Induces Widespread Epigenetic Reprogramming Which Involves Demethylation of Specific Genes. *Carcinogenesis* **2007**, *28*, 560–571. [[CrossRef](#)]
48. Veronezi, G.M.B.; Felisbino, M.B.; Gatti, M.S.V.; Mello, M.L.S.; De Vidal, B.C. DNA Methylation Changes in Valproic Acid-Treated HeLa Cells as Assessed by Image Analysis, Immunofluorescence and Vibrational Microspectroscopy. *PLoS ONE* **2017**, *12*, e0170740. [[CrossRef](#)]
49. Thangaraju, M.; Ananth, S.; Martin, P.M.; Roon, P.; Smith, S.B.; Sterneck, E.; Prasad, P.D.; Ganapathy, V. C/Ebp δ Null Mouse as a Model for the Double Knock-out of Slc5a8 and Slc5a12 in Kidney. *J. Biol. Chem.* **2006**, *281*, 26769–26773. [[CrossRef](#)]
50. Frank, H.; Gröger, N.; Diener, M.; Becker, C.; Braun, T.; Boettger, T. Lactaturia and Loss of Sodium-Dependent Lactate Uptake in the Colon of SLC5A8-Deficient Mice. *J. Biol. Chem.* **2008**, *283*, 24729–24737. [[CrossRef](#)]
51. Singh, N.; Thangaraju, M.; Prasad, P.D.; Martin, P.M.; Lambert, N.A.; Boettger, T.; Offermanns, S.; Ganapathy, V. Blockade of Dendritic Cell Development by Bacterial Fermentation Products Butyrate and Propionate through a Transporter (Slc5a8)-Dependent Inhibition of Histone Deacetylases. *J. Biol. Chem.* **2010**, *285*, 27601–27608. [[CrossRef](#)]
52. Zimmerman, M.A.; Singh, N.; Martin, P.M.; Thangaraju, M.; Ganapathy, V.; Waller, J.L.; Shi, H.; Robertson, K.D.; Munn, D.H.; Liu, K. Butyrate Suppresses Colonic Inflammation through HDAC1-Dependent Fas Upregulation and Fas-Mediated Apoptosis of T Cells. *Am. J. Physiol.-Gastrointest. Liver Physiol.* **2012**, *302*, 1405–1415. [[CrossRef](#)]
53. Savino, W.; Durães, J.; Maldonado-Galdeano, C.; Perdigon, G.; Mendes-da-Cruz, D.A.; Cuervo, P. Thymus, Undernutrition, and Infection: Approaching Cellular and Molecular Interactions. *Front. Nutr.* **2022**, *9*, 948488. [[CrossRef](#)]
54. Stanevičiūtė, J.; Juknevičienė, M.; Balnyte, I.; Valančiūtė, A.; Lesauskaite, V.; Fadejeva, J.; Stakauskas, R.; Stakišaitis, D. Gender-Related Effect of Sodium Dichloroacetate on the Number of Hassall's Corpuscles and RNA NKCC1 Expression in Rat Thymus. *Biomed Res. Int.* **2019**, *2019*, 1602895. [[CrossRef](#)] [[PubMed](#)]

55. Juknevičienė, M.; Balnytė, I.; Valančiūtė, A.; Lesauskaitė, V.; Stanevičiūtė, J.; Curkūnavičiūtė, R.; Stakišaitis, D. Valproic Acid Inhibits NA-K-2CL Cotransporter RNA Expression in Male but Not in Female Rat Thymocytes. *Dose-Response* **2019**, *17*, 1–8. [[CrossRef](#)] [[PubMed](#)]
56. Livak, K.J.; Schmittgen, T.D. Analysis of Relative Gene Expression Data Using Real-Time Quantitative PCR and the 2- $\Delta\Delta$ CT Method. *Methods* **2001**, *25*, 402–408. [[CrossRef](#)] [[PubMed](#)]
57. Ewels, P.; Magnusson, M.; Lundin, S.; Käller, M. MultiQC: Summarize Analysis Results for Multiple Tools and Samples in a Single Report. *Bioinformatics* **2016**, *32*, 3047–3048. [[CrossRef](#)]
58. Martin, M. Cutadapt Removes Adapter Sequences from High-Throughput Sequencing Reads. *EMBnet. J.* **2011**, *17*, 10–12. [[CrossRef](#)]
59. Cunningham, F.; Allen, J.E.; Allen, J.; Alvarez-Jarreta, J.; Amode, M.R.; Armean, I.M.; Austine-Orimoloye, O.; Azov, A.G.; Barnes, I.; Bennett, R.; et al. Ensembl 2022. *Nucleic Acids Res.* **2022**, *50*, 988–995. [[CrossRef](#)]
60. Dobin, A.; Davis, C.A.; Schlesinger, F.; Drenkow, J.; Zaleski, C.; Jha, S.; Batut, P.; Chaisson, M.; Gingeras, T.R. STAR: Ultrafast Universal RNA-Seq Aligner. *Bioinformatics* **2013**, *29*, 15–21. [[CrossRef](#)]
61. Liao, Y.; Smyth, G.K.; Shi, W. FeatureCounts: An Efficient General Purpose Program for Assigning Sequence Reads to Genomic Features. *Bioinformatics* **2014**, *30*, 923–930. [[CrossRef](#)] [[PubMed](#)]
62. Love, M.I.; Huber, W.; Anders, S. Moderated Estimation of Fold Change and Dispersion for RNA-Seq Data with DESeq2. *Genome Biol.* **2014**, *15*, 550. [[CrossRef](#)] [[PubMed](#)]
63. Sherman, B.T.; Hao, M.; Qiu, J.; Jiao, X.; Baseler, M.W.; Lane, H.C.; Imamichi, T.; Chang, W. DAVID: A Web Server for Functional Enrichment Analysis and Functional Annotation of Gene Lists (2021 Update). *Nucleic Acids Res.* **2022**, *50*, 216–221. [[CrossRef](#)]
64. Huang, D.W.; Sherman, B.T.; Lempicki, R.A. Systematic and Integrative Analysis of Large Gene Lists Using DAVID Bioinformatics Resources. *Nat. Protoc.* **2009**, *4*, 44–57. [[CrossRef](#)] [[PubMed](#)]
65. Wu, T.; Hu, E.; Xu, S.; Chen, M.; Guo, P.; Dai, Z.; Feng, T.; Zhou, L.; Tang, W.; Zhan, L.; et al. ClusterProfiler 4.0: A Universal Enrichment Tool for Interpreting Omics Data. *Innovation* **2021**, *2*, 100141. [[CrossRef](#)] [[PubMed](#)]
66. Ciofani, M.; Zúñiga-Pflücker, J.C. The Thymus as an Inductive Site for T Lymphopoiesis. *Annu. Rev. Cell Dev. Biol.* **2007**, *23*, 463–493. [[CrossRef](#)]
67. Savino, W.; Mendes-Da-Cruz, D.A.; Lepletier, A.; Dardenne, M. Hormonal Control of T-Cell Development in Health and Disease. *Nat. Rev. Endocrinol.* **2016**, *12*, 77–89. [[CrossRef](#)] [[PubMed](#)]
68. Valančiūtė, A.; Mozuraite, R.; Balnytė, I.; Didžiapetriene, J.; Matusevičius, P.; Stakišaitis, D. Sodium Valproate Effect on the Structure of Rat Glandule Thymus: Gender-Related Differences. *Exp. Toxicol. Pathol.* **2015**, *67*, 399–406. [[CrossRef](#)]
69. Sebastianelli, M.; Forte, C.; Galarini, R.; Gobbi, M.; Pistidda, E.; Moncada, C.; Cannizzo, F.T.; Pezzolato, M.; Bozzetta, E.; Cenci-Goga, B.T.; et al. LC-MS/MS Analyses of Bile and Histological Analyses of Thymus as Diagnostic Tools to Detect Low Dose Dexamethasone Illicit Treatment in Beef Cattle at Slaughterhouse. *Steroids* **2020**, *160*, 108671. [[CrossRef](#)]
70. Asghar, A.; Syed, Y.M.; Nafis, F.A. Polymorphism of Hassall’s Corpuscles in Thymus of Human Fetuses. *Int. J. Appl. Basic Med. Res.* **2012**, *2*, 7–10. [[CrossRef](#)]
71. Hale, L.P.; Markert, M.L. Corticosteroids Regulate Epithelial Cell Differentiation and Hassall Body Formation in the Human Thymus. *J. Immunol.* **2004**, *172*, 617–624. [[CrossRef](#)] [[PubMed](#)]
72. Kadouri, N.; Nevo, S.; Goldfarb, Y.; Abramson, J. Thymic Epithelial Cell Heterogeneity: TEC by TEC. *Nat. Rev. Immunol.* **2020**, *20*, 239–253. [[CrossRef](#)] [[PubMed](#)]
73. Wang, X.; Laan, M.; Bichele, R.; Kisand, K.; Scott, H.S.; Peterson, P. Post-Aire Maturation of Thymic Medullary Epithelial Cells Involves Selective Expression of Keratinocyte-Specific Autoantigens. *Front. Immunol.* **2012**, *3*, 19. [[CrossRef](#)] [[PubMed](#)]
74. Smith, S.M.; Ossa-Gomez, L.J. A Quantitative Histologic Comparison of the Thymus in 100 Healthy and Diseased Adults. *Am. J. Clin. Pathol.* **1981**, *76*, 657–665. [[CrossRef](#)]
75. Skogberg, G.; Lundberg, V.; Lindgren, S.; Gudmundsdóttir, J.; Sandström, K.; Kämpe, O.; Annerén, G.; Gustafsson, J.; Sunnegårdh, J.; van der Post, S.; et al. Altered Expression of Autoimmune Regulator in Infant Down Syndrome Thymus, a Possible Contributor to an Autoimmune Phenotype. *J. Immunol.* **2014**, *193*, 2187–2195. [[CrossRef](#)]
76. Wang, J.; Sekai, M.; Matsui, T.; Fujii, Y.; Matsumoto, M.; Takeuchi, O.; Minato, N.; Hamazaki, Y. Hassall’s Corpuscles with Cellular-Senescence Features Maintain IFN α Production through Neutrophils and PDC Activation in the Thymus. *Int. Immunol.* **2019**, *31*, 127–139. [[CrossRef](#)] [[PubMed](#)]
77. Yano, M.; Kuroda, N.; Han, H.; Meguro-Horike, M.; Nishikawa, Y.; Kiyonari, H.; Maemura, K.; Yanagawa, Y.; Obata, K.; Takahashi, S.; et al. Aire Controls the Differentiation Program of Thymic Epithelial Cells in the Medulla for the Establishment of Self-Tolerance. *J. Exp. Med.* **2008**, *205*, 2827–2838. [[CrossRef](#)] [[PubMed](#)]
78. Watanabe, N.; Wang, Y.H.; Lee, H.K.; Ito, T.; Wang, Y.H.; Cao, W.; Liu, Y.J. Hassall’s Corpuscles Instruct Dendritic Cells to Induce CD4⁺ CD25⁺ Regulatory T Cells in Human Thymus. *Nature* **2005**, *436*, 1181–1185. [[CrossRef](#)]
79. Besin, G.; Gaudreau, S.; Menard, M.; Guindi, C.; Dupuis, G.; Amrani, A. Thymic Stromal Lymphopoietin and Thymic Stromal Lymphopoietin-Conditioned Dendritic Cells Induce Regulatory T-Cell Differentiation and Protection of NOD Mice against Diabetes. *Diabetes* **2008**, *57*, 2107–2117. [[CrossRef](#)]
80. Laan, M.; Salumets, A.; Klein, A.; Reintamm, K.; Bichele, R.; Peterson, H.; Peterson, P. Post-Aire Medullary Thymic Epithelial Cells and Hassall’s Corpuscles as Inducers of Tonic Pro-Inflammatory Microenvironment. *Front. Immunol.* **2021**, *12*, 635569. [[CrossRef](#)]

81. Bhutia, Y.D.; Babu, E.; Ramachandran, S.; Yang, S.; Thangaraju, M.; Ganapathy, V. SLC Transporters as a Novel Class of Tumour Suppressors: Identity, Function and Molecular Mechanisms. *Biochem. J.* **2016**, *473*, 1113–1124. [[CrossRef](#)]
82. Babu, E.; Ramachandran, S.; Coothankandaswamy, V.; Elangovan, S.; Prasad, P.D.; Ganapathy, V.; Thangaraju, M. Role of SLC5A8, a Plasma Membrane Transporter and a Tumor Suppressor, in the Antitumor Activity of Dichloroacetate. *Oncogene* **2011**, *30*, 4026–4037. [[CrossRef](#)] [[PubMed](#)]
83. Liu, S.; Zhao, S.; Cheng, Z.; Ren, Y.; Shi, X.; Mu, J.; Ge, X.; Dai, Y.; Li, L.; Zhang, Z. Akkermansia Muciniphila Protects against Antibiotic-Associated Diarrhea in Mice. *Probiot. Antimicrob. Proteins* **2023**, *15*, 1–15. [[CrossRef](#)] [[PubMed](#)]
84. Damanskienė, E.; Balnytė, I.; Valančiūtė, A.; Alonso, M.M.; Stakišaitis, D. Different Effects of Valproic Acid on SLC12A2, SLC12A5 and SLC5A8 Gene Expression in Pediatric Glioblastoma Cells as an Approach to Personalised Therapy. *Biomedicines* **2022**, *10*, 968. [[CrossRef](#)] [[PubMed](#)]
85. Colantonio, A.D.; Epeldegui, M.; Jesiak, M.; Jachimowski, L.; Blom, B.; Uittenbogaart, C.H. IFN- α Is Constitutively Expressed in the Human Thymus, but Not in Peripheral Lymphoid Organs. *PLoS ONE* **2011**, *6*, e24252. [[CrossRef](#)]
86. Lienenklaus, S.; Cornitescu, M.; Ziętara, N.; Łyszkiewicz, M.; Gekara, N.; Jabłońska, J.; Edenhofer, F.; Rajewsky, K.; Bruder, D.; Hafner, M.; et al. Novel Reporter Mouse Reveals Constitutive and Inflammatory Expression of IFN- β In Vivo. *J. Immunol.* **2009**, *183*, 3229–3236. [[CrossRef](#)]
87. Trampont, P.C.; Tosello-Trampont, A.C.; Shen, Y.; Duley, A.K.; Sutherland, A.E.; Bender, T.P.; Littman, D.R.; Ravichandran, K.S. CXCR4 Acts as a Costimulator during Thymic B-Selection. *Nat. Immunol.* **2010**, *11*, 162–170. [[CrossRef](#)]
88. Annunziato, F.; Romagnani, P.; Cosmi, L.; Lazzeri, E.; Romagnani, S. Chemokines and Lymphopoiesis in Human Thymus. *Trends Immunol.* **2001**, *22*, 277–281. [[CrossRef](#)]
89. Campbell, J.J.; Pan, J.; Butcher, E.C. Cutting Edge: Developmental Switches in Chemokine Responses during T Cell Maturation. *J. Immunol.* **1999**, *163*, 2353–2357. [[CrossRef](#)]
90. Leite-de-Moraes, M.C.; Hontebeyrie-Joskowicz, M.; Dardenne, M.; Savino, W. Modulation of Thymocyte Subsets during Acute and Chronic Phases of Experimental Trypanosoma Cruzi Infection. *Immunology* **1992**, *77*, 95–98.
91. Korn, T.; Hiltensperger, M. Role of IL-6 in the Commitment of T Cell Subsets. *Cytokine* **2021**, *146*, 155654. [[CrossRef](#)] [[PubMed](#)]
92. Balcells, F.; Martínez Monteros, M.J.; Gómez, A.L.; Cazorla, S.I.; Perdígón, G.; Maldonado-Galdeano, C. Probiotic Consumption Boosts Thymus in Obesity and Senescence Mouse Models. *Nutrients* **2022**, *14*, 616. [[CrossRef](#)] [[PubMed](#)]
93. Hosokawa, H.; Rothenberg, E.V. Cytokines, Transcription Factors, and the Initiation of T-Cell Development. *Cold Spring Harb. Perspect. Biol.* **2018**, *10*, a028621. [[CrossRef](#)] [[PubMed](#)]
94. Palomino, D.C.; Marti, L.C. Chemokines and Immunity. *Einstein* **2015**, *13*, 469–473. [[CrossRef](#)] [[PubMed](#)]
95. Ren, M.; Zhang, J.; Dai, S.; Wang, C.; Chen, Z.; Zhang, S.; Xu, J.; Qin, X.; Liu, F. CX3CR1 Deficiency Exacerbates Immune-Mediated Hepatitis by Increasing NF- κ B-Mediated Cytokine Production in Macrophage and T Cell. *Exp. Biol. Med.* **2023**, *248*, 117–129. [[CrossRef](#)] [[PubMed](#)]
96. Griffith, J.W.; Sokol, C.L.; Luster, A.D. Chemokines and Chemokine Receptors: Positioning Cells for Host Defense and Immunity. *Annu. Rev. Immunol.* **2014**, *32*, 659–702. [[CrossRef](#)] [[PubMed](#)]
97. Gaffen, S.L. Structure and Signalling in the IL-17 Receptor Family. *Nat. Rev. Immunol.* **2009**, *9*, 556–567. [[CrossRef](#)] [[PubMed](#)]
98. Bocker, C.; Thompson, D.; Matsumoto, A.; Nebert, D.W.; Vasiliou, V. Evolutionary Divergence and Functions of the Human Interleukin (IL) Gene Family. *Hum. Genomics* **2010**, *5*, 30–55. [[CrossRef](#)]
99. Matsubara, E.; Yano, H.; Pan, C.; Komohara, Y.; Fujiwara, Y.; Zhao, S.; Shinchi, Y.; Kurotaki, D.; Suzuki, M. The Significance of SPP1 in Lung Cancers and Its Impact as a Marker for Protumor Tumor-Associated Macrophages. *Cancers* **2023**, *15*, 2250. [[CrossRef](#)]
100. MacDonald, L.; Alivernini, S.; Tolusso, B.; Elmesmari, A.; Somma, D.; Perniola, S.; Paglionico, A.; Petricca, L.; Bosello, S.L.; Carfi, A.; et al. COVID-19 and RA Share an SPP1 Myeloid Pathway That Drives PD-L1+ Neutrophils and CD14+ Monocytes. *JCI Insight* **2021**, *6*, e147413. [[CrossRef](#)]
101. Naito, T.; Ise, M.; Tanaka, Y.; Kohwi-Shigematsu, T.; Kondo, M. Crucial Roles of SATB1 in Regulation of Thymocyte Migration after Positive Selection. *J. Immunol.* **2023**, *211*, 209–218. [[CrossRef](#)] [[PubMed](#)]
102. Kondělková, K.; Vokurková, D.; Krejsek, J.; Borská, L.; Fiala, Z.; Ctírad, A. Regulatory T Cells (TREG) and Their Roles in Immune System with Respect to Immunopathological Disorders. *Acta Medica* **2010**, *53*, 73–77. [[CrossRef](#)]
103. Alkharsah, K.R. VEGF Upregulation in Viral Infections and Its Possible Therapeutic Implications. *Int. J. Mol. Sci.* **2018**, *19*, 1642. [[CrossRef](#)] [[PubMed](#)]
104. Zhao, S.Q.; Li, J.M. G-CSF and Its Receptor in Hematopoiesis. *Zhongguo Shi Yan Xue Ye Xue Za Zhi* **2015**, *23*, 871–877. [[PubMed](#)]
105. Dharra, R.; Kumar Sharma, A.; Datta, S. Emerging Aspects of Cytokine Storm in COVID-19: The Role of Proinflammatory Cytokines and Therapeutic Prospects. *Cytokine* **2023**, *169*, 156287. [[CrossRef](#)]
106. Wang, H.; FitzPatrick, M.; Wilson, N.J.; Anthony, D.; Reading, P.C.; Satzke, C.; Dunne, E.M.; Licciardi, P.V.; Seow, H.J.; Nichol, K.; et al. CSF3R/CD114 Mediates Infection-Dependent Transition to Severe Asthma. *J. Allergy Clin. Immunol.* **2019**, *143*, 785–788. [[CrossRef](#)] [[PubMed](#)]
107. Wang, H.; Aloe, C.; Wilson, N.; Bozinovski, S. G-CSFR Antagonism Reduces Neutrophilic Inflammation during Pneumococcal and Influenza Respiratory Infections without Compromising Clearance. *Sci. Rep.* **2019**, *9*, 17732. [[CrossRef](#)] [[PubMed](#)]
108. Takatsuka, H.; Takemoto, Y.; Mori, A.; Okamoto, T.; Kanamaru, A.; Kakishita, E. Common Features in the Onset of ARDS after Administration of Granulocyte Colony-Stimulating Factor. *Chest* **2002**, *121*, 1716–1720. [[CrossRef](#)] [[PubMed](#)]

109. Sameni, M.; Mirmotalebisohi, S.A.; Dadashkhan, S.; Ghani, S.; Abbasi, M.; Noori, E.; Zali, H. COVID-19: A Novel Holistic Systems Biology Approach to Predict Its Molecular Mechanisms (In Vitro) and Repurpose Drugs. *DARU J. Pharm. Sci.* **2023**, *31*, 155–171. [[CrossRef](#)]
110. Gould, S.E.; Day, M.; Jones, S.S.; Doral, H. Bmp-7 Regulates Chemokine, Cytokine, and Hemodynamic Gene Expression in Proximal Tubule Cells. *Kidney Int.* **2002**, *61*, 51–60. [[CrossRef](#)]
111. Singla, D.K.; Singla, R.; Wang, J. BMP-7 Treatment Increases M2 Macrophage Differentiation and Reduces Inflammation and Plaque Formation in Apo E^{-/-} Mice. *PLoS ONE* **2016**, *11*, e0147897. [[CrossRef](#)] [[PubMed](#)]
112. Alves, N.L.; Arosa, F.A.; van Lier, R.A.W. Common γ Chain Cytokines: Dissidence in the Details. *Immunol. Lett.* **2007**, *108*, 113–120. [[CrossRef](#)] [[PubMed](#)]
113. Rochman, Y.; Spolski, R.; Leonard, W.J. New Insights into the Regulation of T Cells by Γ c Family Cytokines. *Nat. Rev. Immunol.* **2009**, *9*, 480–490. [[CrossRef](#)]
114. Collison, L.W.; Vignali, D.A.A. Interleukin-35: Odd One out or Part of the Family? *Immunol. Rev.* **2008**, *226*, 248–262. [[CrossRef](#)] [[PubMed](#)]
115. Kinsella, S.; Dudakov, J.A. When the Damage Is Done: Injury and Repair in Thymus Function. *Front. Immunol.* **2020**, *11*, 1745. [[CrossRef](#)]
116. Oshio, T.; Komine, M.; Tsuda, H.; Tominaga, S.I.; Saito, H.; Nakae, S.; Ohtsuki, M. Nuclear Expression of IL-33 in Epidermal Keratinocytes Promotes Wound Healing in Mice. *J. Dermatol. Sci.* **2017**, *85*, 106–114. [[CrossRef](#)] [[PubMed](#)]
117. Mencarelli, A.; Cipriani, S.; Francisci, D.; Santucci, L.; Baldelli, F.; Distrutti, E.; Fiorucci, S. Highly Specific Blockade of CCR5 Inhibits Leukocyte Trafficking and Reduces Mucosal Inflammation in Murine Colitis. *Sci. Rep.* **2016**, *6*, 30802. [[CrossRef](#)]
118. Cayrol, C.; Girard, J.P. Interleukin-33 (IL-33): A Critical Review of Its Biology and the Mechanisms Involved in Its Release as a Potent Extracellular Cytokine. *Cytokine* **2022**, *156*, 155891. [[CrossRef](#)]
119. Koh, S.S.; Ooi, S.C.Y.; Lui, N.M.Y.; Qiong, C.; Ho, L.T.Y.; Cheah, I.K.M.; Halliwell, B.; Herr, D.R.; Ong, W.Y. Effect of Ergothioneine on 7-Ketocholesterol-Induced Endothelial Injury. *Neuro Mol. Med.* **2021**, *23*, 184–198. [[CrossRef](#)]
120. Gutierrez, L.S.; Lopez-Dee, Z.; Pidcock, K. Thrombospondin-1: Multiple Paths to Inflammation. *Mediat. Inflamm.* **2011**, *2011*, 296069.
121. Hamldar, S.; Kiani, S.J.; Khoshmirasafa, M.; Nahand, J.S.; Mirzaei, H.; Khatami, A.R.; Kahyesh-Esfandiary, R.; Khanaliha, K.; Tavakoli, A.; Babakhaniyan, K.; et al. Expression Profiling of Inflammation-Related Genes Including IFI-16, NOTCH2, CXCL8, THBS1 in COVID-19 Patients. *Biologicals* **2022**, *80*, 27–34. [[CrossRef](#)] [[PubMed](#)]
122. Zhang, L.; Zhang, Q.; Wang, H.; Feng, P.; Yang, G.; Yang, L. Effects of Early Pregnancy on the Complement System in the Ovine Thymus. *Vet. Res. Commun.* **2022**, *46*, 137–145. [[CrossRef](#)] [[PubMed](#)]
123. Nakayama, Y.; Kim, S.-I.; Kim, E.H.; Lambris, J.D.; Sandor, M.; Suresh, M. C3 Promotes Expansion of CD8⁺ and CD4⁺ T Cells in a *Listeria Monocytogenes* Infection. *J. Immunol.* **2009**, *183*, 2921–2931. [[CrossRef](#)] [[PubMed](#)]
124. Sahu, S.K.; Ozantürk, A.N.; Kulkarni, D.H.; Ma, L.; Barve, R.A.; Dannull, L.; Lu, A.; Starick, M.; McPhatter, J.; Garnica, L.; et al. Lung Epithelial Cell-derived C3 Protects against Pneumonia-Induced Lung Injury. *Sci. Immunol.* **2023**, *8*, eabp9547. [[CrossRef](#)]
125. Nagasubramanian, K.; Jha, S.; Rathore, A.S.; Gupta, K. Identification of Small Molecule Modulators of Class II Transactivator-I Using Computational Approaches. *J. Biomol. Struct. Dyn.* **2023**, *41*, 8349–8361. [[CrossRef](#)] [[PubMed](#)]
126. Forlani, G.; Shallak, M.; Gatta, A.; Shaik, A.K.B.; Accolla, R.S. The NLR Member CIITA: Master Controller of Adaptive and Intrinsic Immunity and Unexpected Tool in Cancer Immunotherapy. *Biomed. J.* **2023**, *46*, 100631. [[CrossRef](#)] [[PubMed](#)]
127. Provoost, S.; De Grove, K.C.; Fraser, G.L.; Lannoy, V.J.; Tournoy, K.G.; Brusselle, G.G.; Maes, T.; Joos, G.F. Pro- and Anti-Inflammatory Role of ChemR23 Signaling in Pollutant-Induced Inflammatory Lung Responses. *J. Immunol.* **2016**, *196*, 1882–1890. [[CrossRef](#)]
128. Mannes, P.Z.; Barnes, C.E.; Biermann, J.; Latoche, J.D.; Day, K.E.; Zhu, Q.; Tabary, M.; Xiong, Z.; Nedrow, J.R.; Izar, B.; et al. Molecular Imaging of Chemokine-like Receptor 1 (CMKLR1) in Experimental Acute Lung Injury. *Proc. Natl. Acad. Sci. USA* **2023**, *120*, e2216458120. [[CrossRef](#)]
129. Bondue, B.; Vosters, O.; de Nadai, P.; Glineur, S.; de Henau, O.; Luangsay, S.; van Gool, F.; Communi, D.; de Vuyst, P.; Desmecht, D.; et al. ChemR23 Dampens Lung Inflammation and Enhances Anti-Viral Immunity in a Mouse Model of Acute Viral Pneumonia. *PLoS Pathog.* **2011**, *7*, e1002358. [[CrossRef](#)]
130. Luangsay, S.; Wittamer, V.; Bondue, B.; De Henau, O.; Rouger, L.; Brait, M.; Franssen, J.-D.; de Nadai, P.; Huaux, F.; Parmentier, M. Mouse ChemR23 Is Expressed in Dendritic Cell Subsets and Macrophages, and Mediates an Anti-Inflammatory Activity of Chemerin in a Lung Disease Model. *J. Immunol.* **2009**, *183*, 6489–6499. [[CrossRef](#)]
131. Zheng, S.Y.; Shao, X.; Qi, Z.; Yan, M.; Tao, M.H.; Wu, X.M.; Zhang, L.; Ma, J.; Li, A.; Chang, M.X. Zebrafish Nos2a Benefits Bacterial Proliferation via Suppressing ROS and Inducing NO Production to Impair the Expressions of Inflammatory Cytokines and Antibacterial Genes. *Fish Shellfish Immunol.* **2023**, *142*, 109178. [[CrossRef](#)] [[PubMed](#)]
132. Andelova, N.; Waczulikova, I.; Kunstek, L.; Talian, I.; Ravingerova, T.; Jasova, M.; Suty, S.; Ferko, M. Dichloroacetate as a Metabolic Modulator of Heart Mitochondrial Proteome under Conditions of Reduced Oxygen Utilization. *Sci. Rep.* **2022**, *12*, 16348. [[CrossRef](#)] [[PubMed](#)]
133. Uzel, G.; Oylumlu, E.; Durmus, L.; Ciraci, C. Duality of Valproic Acid Effects on Inflammation, Oxidative Stress and Autophagy in Human Eosinophilic Cells. *Int. J. Mol. Sci.* **2023**, *24*, 13446. [[CrossRef](#)] [[PubMed](#)]

134. Ahmadian, M.; Suh, J.M.; Hah, N.; Liddle, C.; Atkins, A.R.; Downes, M.; Evans, R.M. Ppar γ Signaling and Metabolism: The Good, the Bad and the Future. *Nat. Med.* **2013**, *19*, 557–566. [[CrossRef](#)] [[PubMed](#)]
135. Mikacenic, C.; Hansen, E.E.; Radella, F.; Gharib, S.A.; Stapleton, R.D.; Wurfel, M.M. Interleukin-17A Is Associated with Alveolar Inflammation and Poor Outcomes in Acute Respiratory Distress Syndrome. *Crit. Care Med.* **2016**, *44*, 496–502. [[CrossRef](#)] [[PubMed](#)]
136. Righetti, R.F.; Dos Santos, T.M.; Camargo, L.D.N.; Barbosa Aristóteles, L.R.C.R.; Fukuzaki, S.; De Souza, F.C.R.; Santana, F.P.R.; De Agrela, M.V.R.; Cruz, M.M.; Alonso-Vale, M.I.C.; et al. Protective Effects of Anti-IL17 on Acute Lung Injury Induced by LPS in Mice. *Front. Pharmacol.* **2018**, *9*, 1021. [[CrossRef](#)] [[PubMed](#)]
137. Xu, Z.; Shi, L.; Wang, Y.; Zhang, J.; Huang, L.; Zhang, C.; Liu, S.; Zhao, P.; Liu, H.; Zhu, L.; et al. Pathological Findings of COVID-19 Associated with Acute Respiratory Distress Syndrome. *Lancet Respir. Med.* **2020**, *8*, 420–422. [[CrossRef](#)]

Disclaimer/Publisher’s Note: The statements, opinions and data contained in all publications are solely those of the individual author(s) and contributor(s) and not of MDPI and/or the editor(s). MDPI and/or the editor(s) disclaim responsibility for any injury to people or property resulting from any ideas, methods, instructions or products referred to in the content.